Coordination Chemistry Reviews 454 (2022) 214344

Contents lists available at ScienceDirect

Coordination Chemistry Reviews

journal homepage: www.elsevier.com/locate/ccr

Review

Polyoxidovanadates' interactions with proteins: An overview

Manuel Aureliano [a,b,*], Nadiia I. Gumerova [c], Giuseppe Sciortino [d], Eugenio Garribba [e], Craig C. McLauchlan [f], Annette Rompel [c,*], Debbie C. Crans [g,*]

[a] Faculdade de Ciências e Tecnologia (FCT), Universidade do Algarve, 8005-139 Faro, Portugal
[b] Centro de Ciências do Mar (CCMar), Universidade do Algarve, 8005-139 Faro, Portugal
[c] Universität Wien, Fakultät für Chemie, Institut für Biophysikalische Chemie, Althanstr. 14, 1090 Vienna, Austria, http://www.bpc.univie.ac.at
[d] Institute of Chemical Research of Catalonia (ICIQ), The Barcelona Institute of Science and Technology, 43007 Tarragona, Spain
[e] Dipartimento di Scienze Mediche, Chirurgiche e Sperimentali, Università di Sassari, I-07100 Sassari, Italy
[f] Department of Chemistry, Illinois State University, Normal, IL 61790-4160, USA
[g] Department of Chemistry and Cell and Molecular Biology Program Colorado State University, Fort Collins, CO 80523, USA

ARTICLE INFO

Article history:
Received 19 August 2021
Received in revised form 10 October 2021
Accepted 29 November 2021
Available online 21 December 2021

This work was written to honor Isabel and José Moura for their great contributions to science.

Keywords:
Polyoxidometalates
Polyoxidovanadates
Decavanadate
Vanadate
Enzymes
Proteins

ABSTRACT

Polyoxidovanadates (POVs, previously named polyoxovanadates) are a subgroup of polyoxidometalates (POMs, previously named polyoxometalates) with interesting pharmacological actions that have been tested as potential antidiabetic, antibacterial, antiprotozoal, antiviral, and anticancer drugs. They contain mainly vanadium and are able to interact with proteins, affecting various biological processes. The most studied POV is the isopolyoxidovanadate decavanadate (V_{10}), which interacts with proteins and/or enzymes such as tyrosine protein phosphatases, P-type ATPases, RNA triphosphatases, myosin and actin. However, in many POVs–protein systems, the binding sites and/or the residues involved in the interaction are not identified. In the present review, the interactions of POVs, as well as linear trivanadate (V_3), both linear and cyclic tetravanadate (V_4) and two proposed heptavanadate (V_7; which are better described by V_{10} molecules), with proteins are described through X-ray crystallographic studies. Interactions with POVs through theoretical and spectroscopic studies of proteins related to muscle contraction, serum, oxidative stress, and diabetes were also discussed. In sum, herein, we describe POVs' interactions with various proteins including acid phosphatase A, receptor tyrosine kinase, ecto-nucleoside triphosphate diphosphohydrolase (NTPDases), transient receptor potential cation channel (TRPM4), phosphoglucomutases, P-type ATPases, myosin, actin, transferrin, albumin, and glucosidases, among others. The putative POVs' effects on proteins are impacted by the POV' stability and speciation. The modes of POVs' interactions include H-bond, electrostatic, H-bond + electrostatic, van der Waals, and covalent binding. The spectroscopic, X-ray and computational results, the sites and modes of binding are described in detail.

Contents

* Corresponding authors at: FCT, Universidade do Algarve, 8005-139 Faro, Portugal. (M. Aureliano).
E-mail addresses: maalves@ualg.pt (M. Aureliano), annette.rompel@univie.ac.at (A. Rompel), debbie.crans@colostate.edu (D.C. Crans).

https://doi.org/10.1016/j.ccr.2021.214344
0010-8545/

Abbreviations

^{51}V-NMR	vanadium-51 NMR
ABC	ATPases, ATP binding-cassette ATPases
AcPA	acid Phosphatase A
ADP	adenosine diphosphate
AMP	adenosine monophosphate
ATP	adenosine triphosphate
BPG	bisphosphoglycerate
CAT	catalase
Ca^{2+}-ATPase	adenosine triphosphatase, calcium dependent
CAN	Ca^{2+} activated, non-selective channel
Cdk	cyclin-dependent kinases
DMAPH	4-dimethylaminopyridinium
DMEM	Dulbecco's modified eagle medium
dPGM	dependent phosphoglycerate mutase
F-actin	filamentous polymerized actin
G-actin	monomeric actin
GSH	reduced glutathione
HSA	human serum albumin
HTf	human serum transferrin
IC_{50}	half maximal inhibitory concentration
MD	molecular docking
MHRs	N-terminal TRPM homology regions
Metf	metformin
NRF2	nuclear factor erythroid 2-related factor 2
NTP	nucleoside triphosphate
NTPDase	ecto-nucleotidetriphosphate diphosphohydrolase
PDB	protein data bank
PG	phosphoglycerate
POM	polyoxidometalate
POMo	polyoxidomolybdate
PONb	polyoxidoniobate
POT	polyoxidotungstate
POV	polyoxidovanadate
ROS	reactive oxygen species
S_1	myosin subfragment 1
SOD	superoxide dismutase
SR	sarcoplasmic reticulum
TEW	tellurium-centered Anderson polyoxidotungstate $[TeW_6O_{24}]^{6-}$
TRP	transient receptor potential channel
TRPM4	transient receptor potential cation channel
UDP	uridine diphosphate
UTP	uridine triphosphate
V_1	monomeric vanadate, simplest oxidovanadate
V_2	dimeric vanadate, divanadate
V_3	trimeric vanadate, trivanadate
V_4	tetrameric vanadate, tetravanadate
V_7	heptameric vanadate, heptavanadate
V_{10}	decameric vanadate, decavanadate
VDAC	voltage-dependent anion-selective channel
vdW	van der Waals

1. Introduction

In the last 30 years, the number of studies of polyoxidometalates (POMs, previously named polyoxometalates) and polyoxidovanadates (POVs, previously named polyoxovanadates) associated with enzymatic inhibition [1–5] and diseases, including insulin enhancement agents [6–9] for diabetes mellitus, and inhibitors of the aggregation of amyloid β-peptides associated with Alzheimer's disease have clearly increased [10,11]. The growing interest in POMs and POVs is extending their applications to diverse areas of basic and applied sciences [12–18] with several studies about various aspects and applications of POVs published covering chemical engineering [19] catalysis [20], environmental chemistry [21], material science [18], biochemistry, biology, pharmacology, and medicine [5,13,14,22–24].

POVs' structures have widespread sizes and shapes and may include other hetero-ions such as P^V and As^V (Fig. 1). The addenda metal oxidoions M=O generally contain M = W^{VI}, Mo^{VI}, and/or V^V and other transition metal ions such as Co^{II}, and/or Mn^{II}. The structures are described in excellent reviews on chemistry of these POV compounds [12,23,25,26].

In the present review, we describe recent studies on the interaction of polyoxidovanadates with proteins, depending on the diversity and nature of the particular POV, and their potential implications in biological processes as well as in biomedical applications. In order to understand such an interaction, information on the stability and speciation under physiological conditions are necessary. In some studies, the protein interactions with other oxidovanadates, such as monomeric (V_1, Fig. 1A), dimeric (V_2, Fig. 1B), trimeric (V_3) and tetrameric (V_4, Fig. 1C, D) vanadates, as well as other POVs were investigated [27]. The effects of vanadium coordination complexes are not the focus of this review, and the reader is referred to other sources for such information [28–32].

2. POVs' stability and speciation

Considering the structural complexity of POVs, their stabilities are variable and it is important to determine what species exist in solution together with the proteins. Hence, it is desired that the stability of the species is investigated under the assay conditions, as recently reviewed [5,33,34].

2.1. Stability of POVs under physiological conditions

Decavanadate, $[V_{10}O_{28}]^{6-}$ (V_{10}, Fig. 1H), is an isopolyoxidovanadate that has been described in detail and serves to showcase the relevance of POVs' speciation and stability to deduce its biological effects [34,35]. Decavanadate has an oblong, compact structure with dimensions of 8.3 × 7.7 × 5.4 Å [36–38]. By ^{51}V NMR

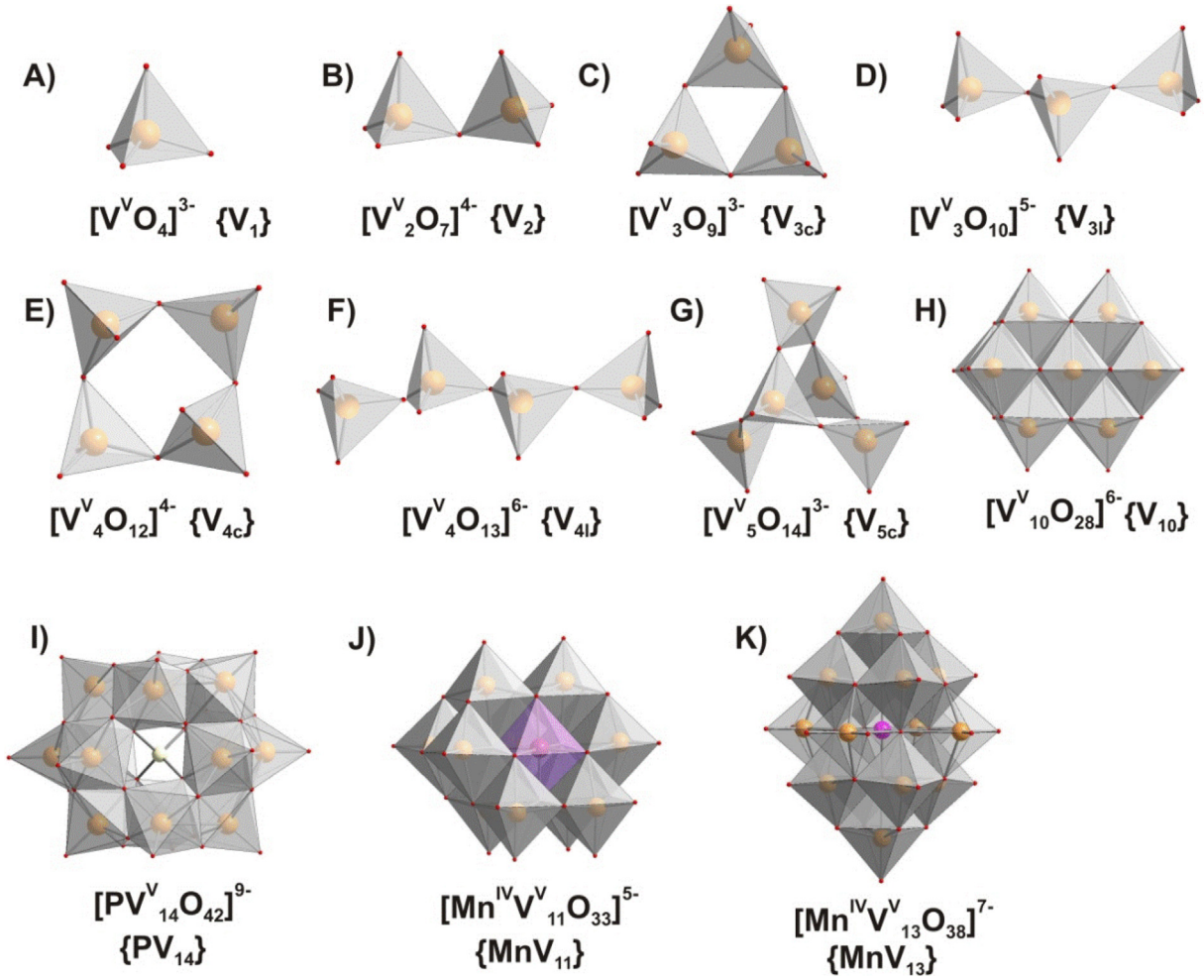

Fig. 1. Oxidovanadates and polyoxidovanadate structures with the nuclearity up to 14 addenda atoms and both tetrahedral and octahedral coordination of V. Tri- and tetravanadates are presented in two forms – cyclic ({V_{3c}}, **C** and {V_{4c}}, **E**) and linear ({V_{3l}}, **D** and {V_{4l}}, **F**). The linear forms of {V_{3l}} and {V_{4l}} have never been obtained in solid state. In the {MnV_{13}} structure, **K**, four equatorial V atoms have 75 % occupancy [27] and so in total correspond to three V ions with full occupancy in the sum formula. Color code: {VO_x}, grey; O, red; P, yellow; Mn, pink. The subscript "c" stands for "cyclic", "l" for "linear". (For interpretation of the references to color in this figure legend, the reader is referred to the web version of this article.)

spectroscopy, three different vanadium ion environments can be distinguished in the V_{10} structure. The yellow or bright orange color of V_{10} solutions can be detected at 360 and 400 nm by UV/Vis spectroscopy [34,39] and the V_{10} stability can be followed by this technique, even for μM concentrations [39,40]. Once formed, V_{10} was shown to be persisting in solution even in the neutral and basic pH range where V_{10} is expected to be no longer thermodynamically stable [34,35]; kinetic reasons can explain this behavior. At acidic pH values, from pH 2 to 6, it is the most stable oxidovanadate. The speciation profile is shown in Fig. 2, illustrating that V_{10} has several protonation states with all the pK_a values falling in the range from pH 2 to 6.

The acidic orange decavanadate solutions can be hydrolyzed by either heating or boiling the neutral or alkaline solutions into the colorless monomeric and oligomeric vanadates [34,41,42]. ^{51}V NMR spectroscopy can be used to monitor the speciation of V_{10} in enzyme assays or in growth media and experiments can be designed to evaluate specific interactions with proteins [5,34,39,40,43,44]. For V_{10}, as well as for other POVs, particularly those that are labile such as V_2 and V_4, respectively, it is possible by combining kinetic with spectroscopic studies to analyze their stability, recognize their specific protein interactions, and determine the specific POV species' contribution to the observed biological effects [34,35,45–48]. In contrast to the labile oxidovanadates, the half-life of decavanadate is much greater and in serum is 15 h

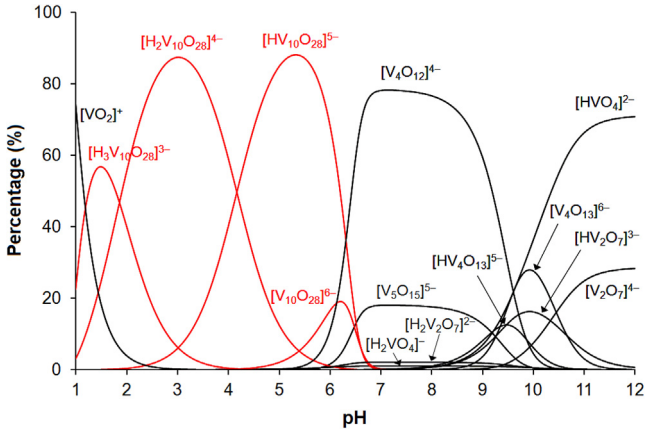

Fig. 2. Aqueous solution species distribution of V(V) as a function of pH at 0.200 M. The stability constants of the inorganic vanadates were taken from [41]. Decavanadate (V_{10}) species are shown in red. (For interpretation of the references to color in this figure legend, the reader is referred to the web version of this article.)

at ambient temperature [39], whereas in buffered media at 25 °C and 37 °C, the half-life decreases to 12 h and 3 h, respectively [39,49]. When V_{10} was applied to media with growth additives for mycobacteria, the half-life reduces even further to a few hours [50]. Metal-based compounds are subject to speciation chemistry [51], which depend on buffers itself and all the other components in the solution, emphasizing the need to confirm the stability of V_{10} under the assay conditions [34,35,39,49,52,53].

The kinetics of the decomposition of sodium and metforminium decavanadate were determined in Dulbecco's modified Eagle's medium (DMEM, $CaCl_2$, 0.2 g/L; KCl, 0.4 g/L; NaCl, 6.4 g/L; Na_2HPO_4, 0.109 g/L; Na_2CO_3, 3.7 g/L; glucose, 1 g/L, and 20 proteinogenic amino acids) at pH 7.4 and 25 °C [54]. In these systems, the results showed that the half-life time of $[H_2VO_4]^-$ (V_1, Fig. 1A) and other smaller oxidovanadates species such as $[H_2V_2O_7]^{2-}$ (V_2, Fig. 1B), $[V_4O_{12}]^{4-}$ (V_4, Fig. 1E) and $[V_5O_{15}]^{5-}$ (V_5) were 9 and 11 h for sodium and metforminium salts, consistent with earlier reports in other growth media and differences in lifetime based on counterion, temperature and, most importantly, pH [55–57].

2.2. Do proteins affect POVs' stability and/or speciation?

Although speciation studies consider all the contributions of components in solution, the effects of proteins are usually neglected [39,53]. The presence of macromolecules can significantly affect, and in some cases increase, the stability of V_{10}. In 2006, it was described that, at pH 7.4, the decavanadate's half-life increases 5.5-fold in the presence of the monomeric form of actin (G-actin) [39], while the addition of *Mycobacterium smegmatis* or *Mycobacterium tuberculosis* cells to a V_{10} solution between pH 5.8 and 6.8 causes immediate decomposition of the decavanadate [50]. Changes in its hydrolytic stability caused by the addition of G-actin is in contrast to the stability of POVs in pure water and illustrate one more time the potential change in the POV's stability through addition of biomolecules [39,50]. Similarly, studies with V_{10} as a phosphatase inhibitor have shown that the enzymes may facilitate hydrolysis [58]. V_{10} is stable for weeks in pure aqueous at pH 4.0 and no change in the hydrolysis rate is observed [59].

3. POVs' interactions with proteins

In the present review we focus on POVs' interactions with proteins, which complements previous reviews on the binding of general vanadium compounds [60,61], polyoxidomolybdates- or polyoxidotungstate-protein binding [1,3,15] and updates previous reviews on V_{10} and other POVs [5,34]. The interactions of POV (summarized in Tables 1 and 2, starting from 1989 for Table 1) with protein can be grouped into:

i) *Coordinative or covalent* interaction of an amino acid side-chain to V(V). This unusual binding type is represented by binding of ß-alanine to $\{V_6O_{24}\}$ [62]. The possibility that this type of bonding does exist is supported by the observation that the presence of V_{10} caused oxidation of Cys374 in F-actin and one of the protein core cysteine residues in G-actin, presumably Cys272 [63,64] (see below in section 3.2). Oxidation of the protein supports a putative POV bond to the protein or intermolecular electron transfer.

ii) *Non-covalent* binding, more common than the *covalent* one, when the interaction occurs through secondary interactions, namely van der Waals (vdW) contacts and hydrogen bonds (H-bonds). This binding mode depends on several factors, such as the electric charge that influences the electrostatic interactions, the shape and volume size that determine the host–guest complementary, and the formation of H-bonds with the terminal oxygens [65,66]. Other variables are pH and ionic strength. The H-bonds are often directed or mediated by H_2O molecules [67]. The majority of the possible binding modes of V_{10} in proteins as well as a summary of the non-covalent interacting amino acids are given in Fig. 3.

Distinguishing *coordinative* from *non-covalent* bond and determining their strength is not a trivial task and computational methods are often necessary [68,69]. On the framework of *non-covalent* binding, several docking software programs offer the opportunity to examine metal–protein interactions [70–73]. In most of the cases, reproducing experimental results requires adjusting the weights of intramolecular and intermolecular H-bonds and vdW

Table 1
POVs interactions with proteins or inhibition of enzymes, *in vitro* studies.

Protein/Enzyme/Effects	POVs (pH of stock solution)	Year	Ref.
Acid phosphatase (human prostate)	V_1 and V_2	1989	[48]
6-phosphogluconate dehydrogenase	V_4	1990	[45]
Glucose-6-phosphate dehydrogenase (*Leuconostoc mesenteroidex*)	V_2 and V_4	1990	[89]
Glycerol-3-phosphate dehydrogenase	V_4 (and possible weak interaction by V_2)	1991	[97]
Superoxide dismutase	V_4	1991	[90]
Purple acid phosphatase (porcine uterine fluid)	V_1 and oxidovanadium(IV) cation VO_2^+	1992	[98]
Fructose 1,6 bisphosphate aldolase (muscle)	V_2 and V_4	1992	[46]
cAMP-dependent protein kinase	V_{10} (7.1)	1997	[91]
DNA-binding protein	V_1 (pH 11) and V_{10} (pH 7.4)	2002	[92]
Methaemoglobin reductase inhibition	V_1 (pH 6.7) and V_{10} (pH 4)	2003	[55]
Myosin/actomyosin ATPase inhibition	V_{10} (pH 4)	2004	[49]
Muscle contraction regulation	V_{10} (pH 4)	2004	[99]
ATP sensitive cation channels	V_{10} (pH 2)	2004	[100]
TRPM4 cation channels	V_{10} (pH 2)	2004	[101]
G-actin polymerization inhibition	V_{10} (pH 4)	2006	[39]
RNA triphosphatase	V_1 (ortho- and meta; pH not specified) and V_{10} (pH not specified)	2006	[102]
P2X receptor antagonist	V_{10} (pH 2)	2006	[103]
Back-door binding to myosin	V_{10} (pH 4)	2007	[104]
Porin (VDAC) modulator	V_{10} (pH not specified)	2007	[105]
Mitochondrial membrane depolarization; changes in the redox steady-state of cytochrome *b* (complex III) Inhibition of mitochondrial oxygen consumption	V_{10} (pH 4)	2007	[106]
G-Actin oxidation and oxidovanadium(IV) formation	V_{10} (pH 4)	2009	[63]
Na^+/K^+-ATPase inhibition	V_{10} (pH not specified)	2009	[107]
Ca^{2+}-ATPase	V_{10} (pH 4)	2012	[56]
Type I Fc epsilon receptor	V_{10} (pH 7.4)	2013	[108]
ATP prevents V_{10} G-actin reduction	V_{10} (pH 4)	2017	[109]
ex-vivo Na^+/K^+-ATPase inhibition coupled with chloride secretion	PV_{14} (Fig. 1I)	2019	[57]
SR Ca^{2+}-ATPase	MnV_{11} (Fig. 1J) MnV_{13} (Fig. 1K)	2019	[110]
Thaumatin, lysozyme, albumin, transferrin	V_{10}, $V_{10}Cu$ (decavanadate coordinated to Cu^{2+}), $V_{10}Co$ (decavanadate coordinated to Co^{2+})	2019	[43]
V_{10}/Nb_{10} G-actin binding sites	V_{10} (pH 4)	2021	[64]

Table 2
Protein complexes with V_{10} and smaller oxidovanadates investigated using X-ray crystallography or cryogenic electron microscopy.

Protein	Source	PDB code	V-cluster	V-precursor added	pH of media	Image/ method	Ref.
Acid Phosphatase A (AcPA)	*Francisella tularensis*	2D1G	Binds V_{10} on surface (Fig. 1H) Binds V_1 in active site	Na_3VO_4	6.0	Fig. 6 / X-ray	[114]
Ecto-nucleoside triphosphate diphosphohydrolase (NTPDase)	*Rattus norvegicus*	3ZX2	V_{10} (Fig. 1H)	Na_3VO_4	4.0	Fig. 7A / X-ray	[119]
NTPDase	*Legionella pneumophila*	4BRH	V_{10} (Fig. 1H)	Na_3VO_4	5.0	Fig. 7B / X-ray	[120]
Tyrosine kinase	*Homo sapiens, Rattus norvegicus*	3GQI	V_{10} (Fig. 1H)	Na_3VO_4	8.0	Fig. 8 / X-ray	[121]
Human transient receptor potential cation channel (TRPM4)	*Homo sapiens*	5WP6	V_{10} (Fig. 1H)	Na_3VO_4	2.0	Fig. 9 / cryo-EM	[126]
Human cell cycle protein cksh1	*Homo sapiens*	1DKT	V_7 in reported model; but the actual cluster binding is V_{10} (Fig. 1H)	$NaVO_3$	7.4	Fig. 10 / X-ray	[113]
Co-factor dependent phosphoglycerate mutase (dPGM)	*E. coli*	1E59	Linear V_4 (Fig. 1F)	$NaVO_3$	8.0	Fig. 11 / X-ray	[129]
C3 exoenzyme	*Clostridium botulinum*	1UZI	Cyclic V_4 (Fig. 1E)	Na_3VO_4	5.5	Fig. 12A / X-ray	[131]
BtuCD protein	*E. coli*	1L7V	Cyclic V_4 (Fig. 1E)	Na_3VO_4	8.0	Fig. 12B / X-ray	[132]
Phosphatase PhoE	*Geobacillus stearothermophilus*	1H2F	Linear V_3 (Fig. 1D)	NH_4VO_3	4.5 and 5.0	Fig. 13 / X-ray	[133]
Uridine phosphorylase	*E. coli*	1RXS	Unlikely isomer V_7, but information not sufficient to determine the cluster	Na_3VO_4	7.5	No Figure shown / X-ray	[117]
Protein-tyrosine phosphatase YopH	*Yersinia*	3F9B	V_2 (Fig. 1B)	Na_3VO_4	7.5	No Figure shown / X-ray	[134]

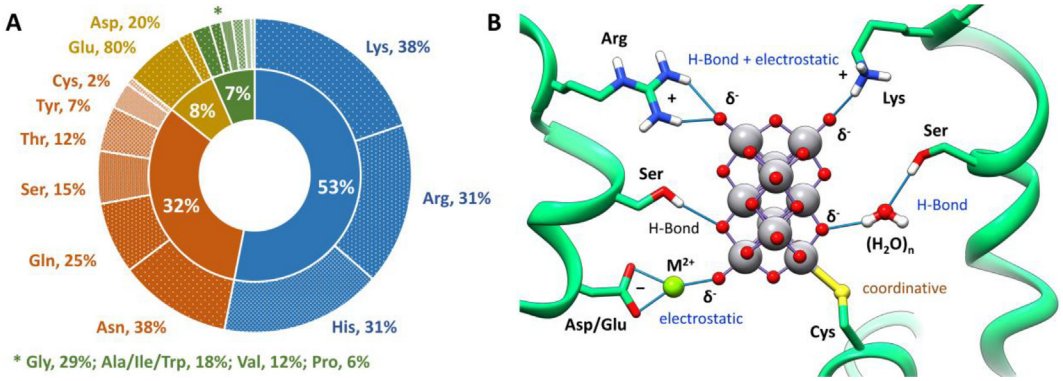

Fig. 3. A) Percentage of amino acids interacting with V_{10} (blue basic, orange polar uncharged, yellow acidic, green unipolar) and B) possible modes of POVs' interaction with proteins. Data taken from ref. [15]. (For interpretation of the references to color in this figure legend, the reader is referred to the web version of this article.)

contacts [74]. The *coordinative* binding can be described with pure electrostatic functions [70–72] or through *covalent docking* approaches nowadays implemented in packages such as GOLD [75] or Autodock [71] and source code modifications such as CovalentDock [76] or Docktite [77]. In these cases, the metal–protein bond needs to be defined *a priori* and restrained during docking. A recently updated version of the *GoldScore* scoring function of the GOLD program was successfully validated for a large series of metal complexes demonstrating its capability to predict coordination bonds without any geometrical constraint or energy restraint [78,79].

A report in 1973 introduced V_{10} as a microMolar inhibitor of rabbit muscle adenylate kinase [80]. These studies were followed by several papers discussing a number of other glycolytic enzymes including fructohexokinase, and phosphofructokinase, among others, all inhibited by V_{10} [5,81–83]. These inhibition studies were complemented early on through ^{51}V NMR studies by Csermely *et al.* in 1985 [84], reporting that the addition of Ca^{2+}-ATPase from the sarcoplasmic reticulum to a solution of both labile oxidovanadates and V_{10} would result in ^{51}V NMR spectra in which V_{10} signals selectively disappeared. These results are consistent with the binding of Ca^{2+}-ATPase to the V_{10} over the simple monooxidovanadates (Fig. 1) [85]. The effects of V_{10} in the structure and function of the Ca^{2+}-ATPase were further explored [85,86]. Thus, it was found that only V_{10} species, and not the V_1 species, were able to inhibit calcium accumulation coupled with ATP hydrolysis [85], as well as proton ejection [86] by the sarcoplasmic reticulum Ca^{2+}-ATPase, clearly affecting energy transduction processes [85–87].

Analysis of the speciation in aqueous solution accompanied the enzyme studies [34,35,46,83–91], and in the case of 6-phosphogluconate dehydrogenase all the observed inhibition could

be attributed to the V_{4c} (Fig. 1E) species [45]. Subsequent kinetic studies confirmed inhibition with corresponding tetranuclear molybdate and ruled out inhibition with the pentanuclear molybdate [88]. Several additional studies with glycolytic enzymes including *Leuconostoc mesenteroidex* glucose-6-phosphate dehydrogenase, glycerol-3-phosphate dehydrogenase, and muscle fructose 1,6-bisphosphate aldolase illustrated that V_{4c} was an inhibitor, although partial inhibition may have been contributed by a weaker inhibiting V_2. The enzyme source can affect the selectivity as illustrated in the case of the *Leishmania* acid phosphatase where both V_{10} and simple monomeric vanadate V_1 were considered to be the inhibitors [2,58], whereas for the human prostatic phosphatase both V_1 and V_2 were inhibitors. These two reports are contrary to most other phosphatases that are inhibited potently by V_1 [93–96]. Besides the ones described above, several studies of the interaction/effects of POVs with proteins/enzymes have been reported since 1989, using kinetic and spectroscopic methods and are summarized in Table 1. Some of the milestones for POVs' interactions with proteins and enzymes are highlighted in a chronological order in Fig. 4.

3.1. X-ray crystallographic studies of POVs with proteins

3.1.1. Overview of V-protein and POV-protein complexes

A search of the Protein Data Bank (PDB) [111,112] on the structures determined by X-ray crystallography using the terms «vanadium», «vanadate», «vanadyl» and «proteins» gives over 150 structures as shown in Fig. 5. This is about 40 structures more than reported in 2015 when an analysis of V-phosphatases complexes was reported [93–96] and a testimony to the increased interest

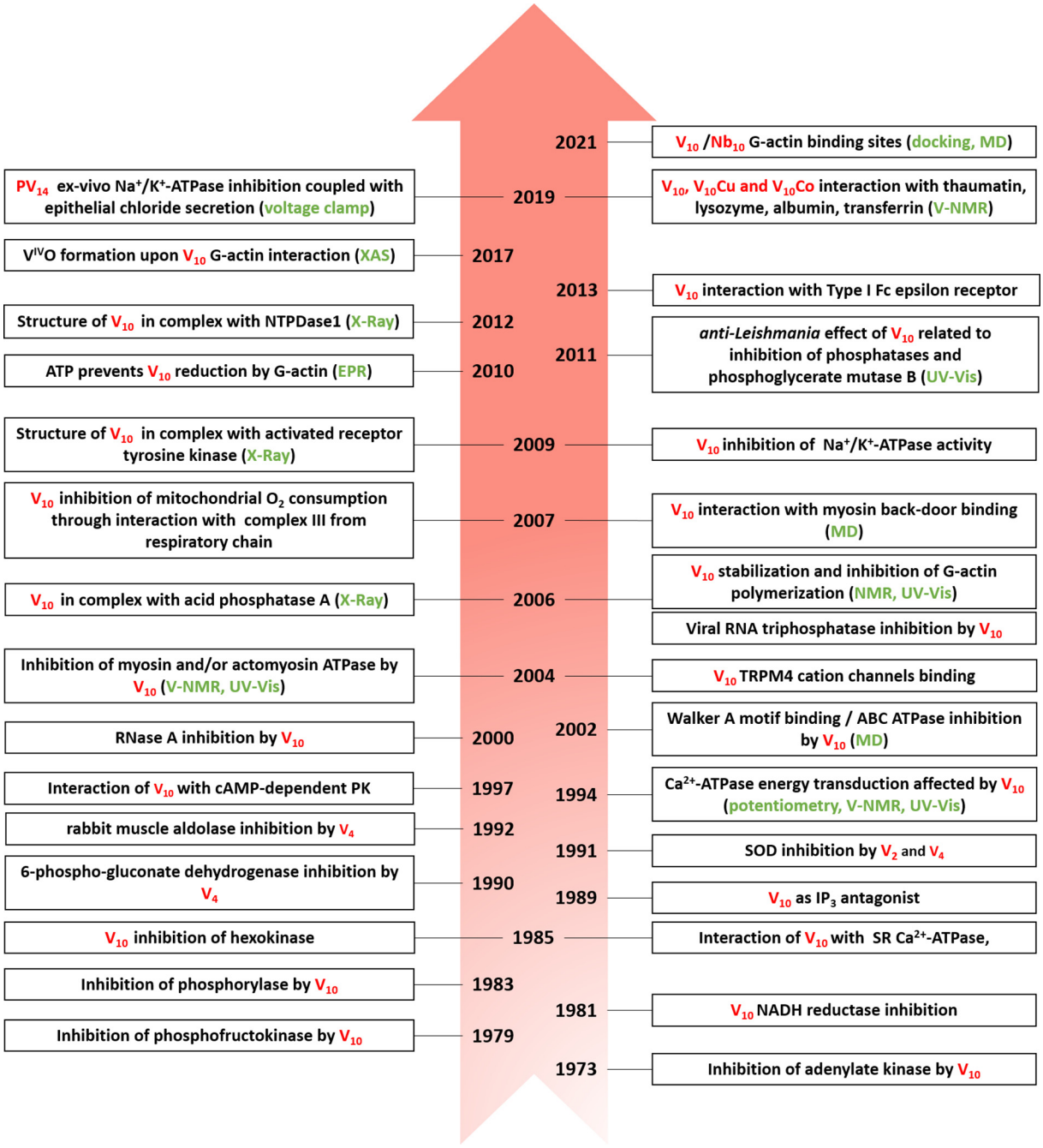

Fig. 4. Timeline for studies of POVs interactions with proteins.

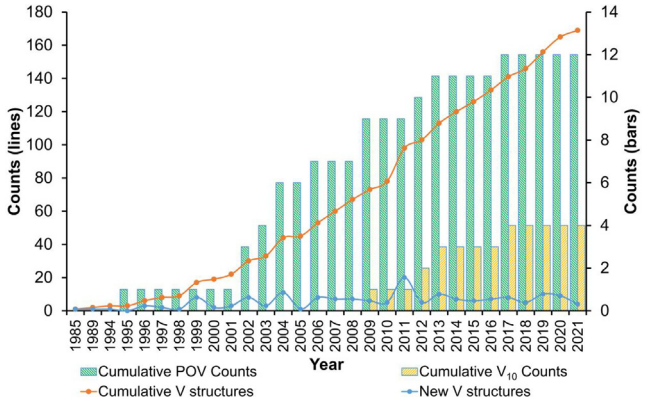

Fig. 5. A plot of POV-proteins complexes reported in the PDB database as a function of time. The right Y-axis relates to the cumulative counts of V_{10}, the left Y-axis describes counts of POVs, cumulative V-structures and new V structures per year.

of V-protein interaction. However, only four structures contain V_{10}, with a fifth structure when cryogenic electron microscopy (cryo-EM) as a technique is used (lined bars, Fig. 5) and a sixth structure where the electron density of the V_{10} is not complete. These six structures include an acid phosphatase, a tyrosine kinase, two ecto-nucleoside triphosphate diphosphohydrolase (NTPDases), a human transient receptor potential cation channel (TRPM4) and a human cell cycle protein CksHs1 [96,111,113–116]. In addition, a few other structures exist containing other POVs (angled bars, Fig. 5), including V_2 (Fig. 1B), V_{3l} (Fig. 1D), V_{4c} (Fig. 1E), and the unusual heptaoxidovanadate (V_7) and are summarized in Table 2. The remaining vanadium-containing protein X-ray structures in the PDB display only one vanadium ion and, although most contain orthovanadate (Fig. 1A) or other protonation states collectively called V_1, some other forms do exist such as V_2 and/or V_4. We first describe the six V_{10}-protein complexes and then the protein adducts with other smaller oxidovanadates including the two species with the binding of V_7 [113,117].

The proteins bind V_1 mainly as tetrahedral and trigonal bipyramidal vanadium oxidoanions; the latter mimic the trigonal bipyramidal transition states of phosphoryl transfer reactions [93,94,96,118]. A few structures in which the binding of the vanadium to a ligand associated with a protein have been reported, along with structures showing the binding of V_{10} or other POVs to the putative active site of the proteins, mimicking the binding of vanadate in place of its endogenous substrate. Specifically, in 2006 the first interaction of V_{10} with the enzyme phosphatase was crystallographically characterized [114]. The enzyme was a respiratory burst-inhibiting acid phosphatase from the Centers for Disease Control and Prevention Category A bio-terrorism agent *Francisella tularensis*. The enzyme is a prototype of a super-family of acid phosphatases and phospholipases C, which was known to be inhibited by vanadate. The phosphatase in question has a serine in the active site as well as a metal ion, but, in contrast to most known phosphatases [93,94], binds V_{10} on the surface [114] and after it V_1 in its active site.

3.1.2. POV-protein complexes: V_{10}-protein adducts

A 2006 publication describes the *Francisella tularensis* Acid phosphatase A (AcPA) as a prototype of a unique superfamily of acid phosphatases and phospholipases C [114]. The phosphatase has in the active site a serine residue interacting with the metal ion through a *coordinative* bond and hence a mechanism that deviates from other phosphatases. In the PDB there is also a structure of *Francisella tularensis* AcPA obtained by crystallization at pH 6.0 bound to V_{10} (PDB code 2D1G) shown in Fig. 6 [114]. This form of the crystal is not described in the publication [114], but the structure is uploaded into the PDB. AcPA is a phosphatase that binds V_1, but V_{10} was observed to also bind to the protein when the enzyme was incubated with vanadate added to the solution in the form of sodium orthovanadate (Na_3VO_4), which converted to V_{10} under the crystallization conditions (pH = 6) [114]. Interestingly, the crystallized protein that binds V_{10} also contains V_1 coordinated in the active site. The larger V_{10} anion is interacting loosely with a group of positively charged amino acids at the surface of the protein. The phosphatase interacts with the V_{10} through several H-bonds resulting in isolation of the V_{10}-protein complex (Fig. 6B). As shown in Fig. 6B, a lysine residue is found to cap the loosely bound V_{10}.

The interaction of V_{10} to the respiratory burst-inhibiting acid phosphatase was not expected because V_1 is clearly the form of vanadate that is known to inhibit other phosphatases [94,93]. However, the inhibition of alkaline phosphatase by V_{10} has also been reported [58]. The inhibition of this phosphatase was different than that observed by V_1 alone, even if the behavior cannot be related to the presence of V_{10} only. In fact, although V_{10} was stable under the conditions of the enzyme assay, some minor hydrolysis of the V_{10} was observed [58]. These observations are consistent with the protein causing the partial hydrolysis of V_{10} to V_1. This latter reaction has been observed for the growth inhibition of *Mycobacterium smegmatus* and *Mycobacteria tuberculosis* where speciation studies showed in both that V_{10} was hydrolyzed more rapidly in media containing the bacteria [44]. Furthermore, growth inhibition of these bacteria was observed by the presence of V_{10} much more potently than by V_1 [44] or similarly by mono-substituted V_{10} derivatives such as V_9Pt and V_9Mo [50].

A second acid phosphatase with a $\{VO_4N\}$ coordination environment is also reported in the PDB (PDB code 4QIH), but has not yet been reported in the literature [115] and, hence, provides little additional insights into the binding of the phosphatase-V systems, but a POV appears to be bound to it. In addition, the human prostatic acid phosphatase was previously reported to be inhibited not only by V_1 but also by the V_2; the former at neutral and basic pH and the latter at acidic pH values (Table 1) [48]. These reports support the interpretation that X-ray data show different oxidovanadates interactions with the prostatic acid phosphatase, depending on the experimental conditions [93,94].

Nucleoside triphosphate diphosphohydrolase 1 (NTPDase1) is an ectonucleotidase that catalyze the hydrolysis of γ- and β-phosphate residues of triphospho- and diphosphonucleosides [116]. By hydrolyzing proinflammatory ATP and platelet-activating ADP to AMP, it blocks platelet aggregation and supports blood flow. NTPDase1 hydrolyzes P2 receptors (P2Y and P2X), such as ATP, ADP, UTP and UDP, with similar efficacy. Investigating the structure and dynamics of this representative member of the eukaryotic NTPDase family was done using a variant of soluble NTPDase1 (PDB codes 4BRH, 3ZX2 and 3GQI for activated receptor) lacking a putative membrane interaction loop between the two lobes of the catalytic domain, as reported by Zebisch *et al.* [119]. Notably, V_{10} was formed under the experimental conditions from orthovanadate. The complex structure of NTPDase1 (PDB code 3ZX2) shows that V_{10} binds electrostatically to a highly positively charged loop that is involved in binding of the nucleobase. The crystal structure shows four independent copies of the protein, each of them bound to V_{10} interacting with the same interfacial active site cleft of the enzyme that contains several lysine groups. As shown in Fig. 7A, the lysine network in the protein interacts through H-bonds with two of the V_{10} faces bringing the two parts of the protein together. Binding on multiple faces of the V_{10} is also observed in the crystal structure of NTPDase1 that bound both thiamine-phosphovanadate and V_{10} (PDB code 4BRH) [120]. V_{10} interacts both with the lysine residues and the NTP unit (Fig. 7B), organizing two parts of the protein around the V_{10} molecule.

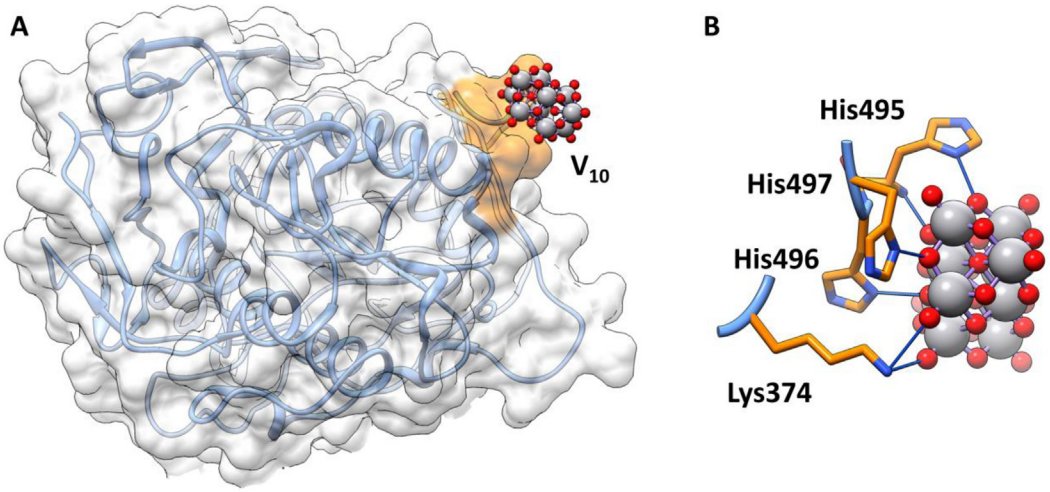

Fig. 6. Structure of *Francisella tularensis* AcPA (PDB code 2D1G) bound to V_{10} (added in form of orthovanadate and converted to V_{10}); A) full protein; B) close-up interaction of protein surface with V_{10} [114].

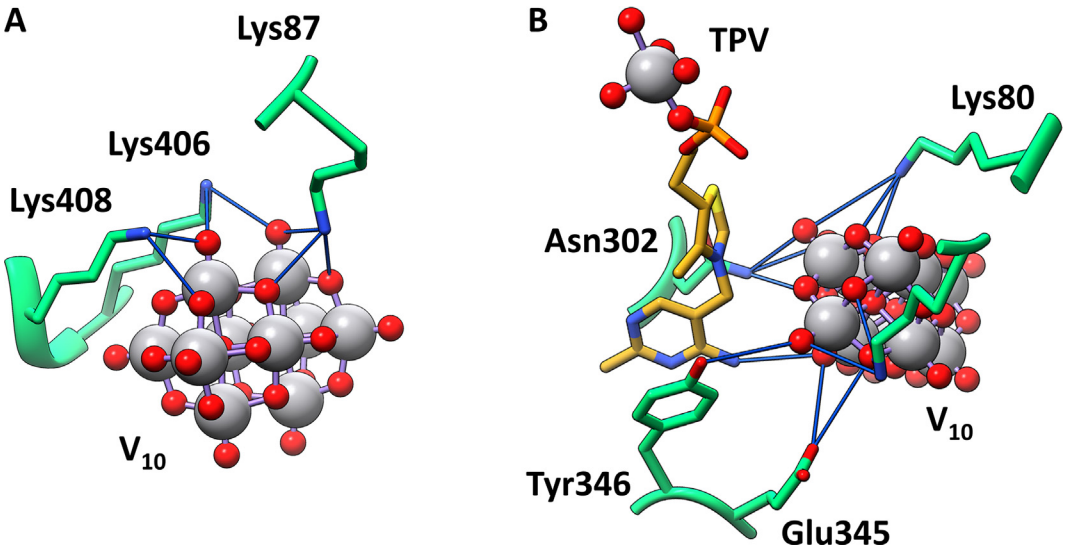

Fig. 7. Close-up view of the X-ray resolved binding sites of V_{10} in: A) apo-NTPDase1 (PDB code 3ZX2) [119]; B) NTPDase1 and thiamine-phosphovanadate (PDB code 4BRH) [120].

V_{10} also binds to an activated receptor tyrosine kinase in one known crystal structure (PDB code 3GQI), shown in Fig. 8 [121]. Although kinases are complementary enzymes to phosphatases which interact strongly with vanadium salts, surprisingly few examples have been reported exhibiting any direct interaction of kinases with vanadate or POVs. The cAMP protein kinase that is removing phosphate groups from peptide substrates and assayed using the Kemptide substrate (Leu-Arg-Arg-Ala-Ser-Leu-Gly) was inhibited by V_{10} [91]. The mechanistic studies demonstrated that the competitive inhibition was caused by the Kemptide binding to the V_{10} anion and not V_{10} binding to the kinase. However, this report proves a rare and strong affinity for a peptide-V_{10} complex which is significantly stronger than the H-bonds observed in the V_{10}-dipeptide (Gly-Gly) complex that is crystallographically characterized [38]. Interaction of the activated receptor tyrosine kinase with V_{10} (PDB code 3GQI) is therefore of great interest [121]. The receptor tyrosine kinase is a subclass of tyrosine kinases and not only a representative of kinases, but a protein involved in mediating cell-to-cell communication and controlling a wide range of complex biological functions, including cell growth, motility, differentiation, and metabolism [122]. V_{10} was previously reported to initiate signaling on another tyrosine kinase receptor, the Type I Fcε receptor [108,123]. This receptor initiates intracellular signaling cascades ultimately leading to degranulation, the release of histamine, from cytoplasmic vesicles, as a key event leading to physical symptoms associated with an allergic response.

In the crystal structure of the activated receptor tyrosine kinase (PDB code 3GQI) the V_{10} moiety is found at a turn on the protein surface and at the interface between PLCγ and FGFR1-3p protein domains [121]. The protein peptides are organized/wrapped around the V_{10} anion (Fig. 8). The authors reported the crystallization in a tris-buffered solution (pH 8.0) containing the protein, where Na_3VO_4 was added. However, the V_{10} anion was localized using idealized V_{10} coordinates placed where high electron density was present in the difference map. The buffered alkaline conditions of the crystallization would not normally favor formation of V_{10}, however in the deposited structure the authors assigned the observed density as V_{10} and optimized the geometry to fit. The V_{10} is found in close contact with a positively charged patch at the interface between FGFR1-3p and PLCγ chains (Fig. 8A) [121].

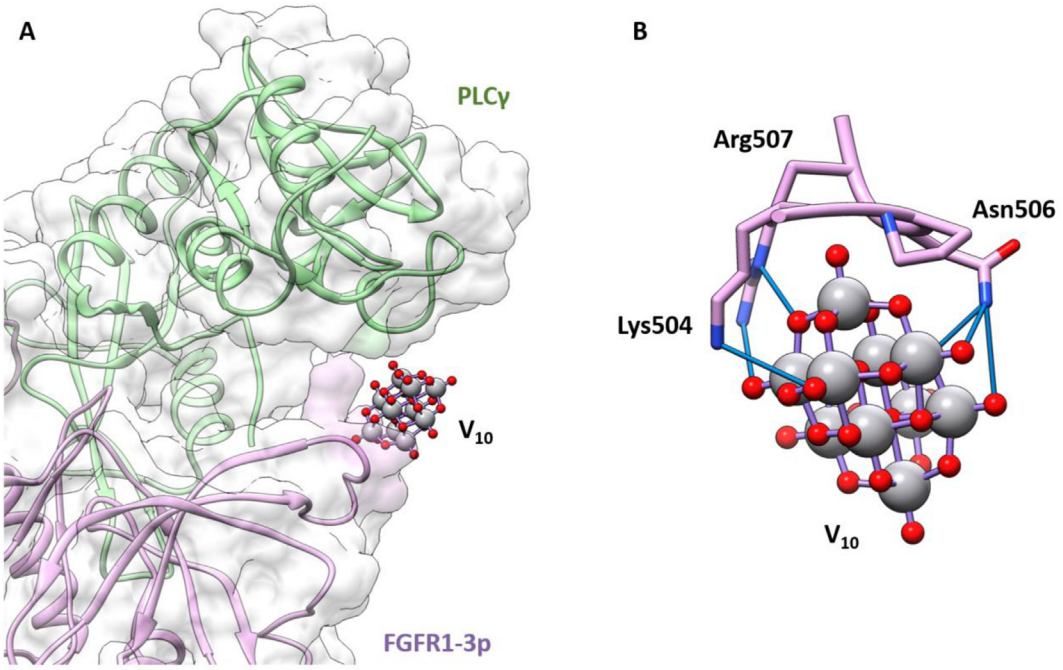

Fig. 8. Tyrosine kinase from activated receptor tyrosine kinase (PDB code 3GQI) [121]. A) interaction of V_{10} at interface between FGFR1-3p and PLCγ chains; B) close view of the V_{10} interaction with the FGFR1-3p chain. H-bond contacts are depicted with blue lines. (For interpretation of the references to color in this figure legend, the reader is referred to the web version of this article.)

Upon closer examination, the V_{10} anion is H-bonding with two adjacent amino acid side chains, namely Asn506 and Arg507, the binding is further supported by Lys504 (Fig. 8B) interacting with a different V_{10} surface part than observed with the apo-NTPDase1, NTPDase1 and thiamine-phosphovanadate shown in Fig. 7; i.e. the protein is interacting with the end of the oblong anisotropic V_{10} anion rather than the side of the V_{10}. Given the difference in binding directionality and the use of idealized coordinates, it is possible that the cluster is actually a number of disordered smaller oxidovanadate ions that are known to form at pH 8 [41,124]. The small number of available protein complexes with V_{10} makes it difficult to label this motif as an outlier. Such interpretation is especially difficult given the similarity in interactions between activated receptor tyrosine kinase (PDB code 3GQI) and the acid phosphatase structure (PDB code 2D1G) shown in Fig. 6. Although protein binding can stabilize V_{10} at higher pH values [39] and some counterions have been found to significantly change fundamental properties of V_{10} [125], we point to the unlikely formation of V_{10} at pH 8, and the existence of an attractive interpretation that the electron density in the protein complex reported in ref. [121] can be attributed to one or more of the smaller rapidly equilibrating oxidovanadates.

Transient receptor potential channel (TRP) is a Ca^{2+}-activated, non-selective cation channel that is permeable to Na^+ and K^+ and is found to depolarize the cell [126]. This process can be modulated by V_{10}. It is one of the eight melastatin-like transient receptor potential (TRPM) subfamily of TRP channels. TRPM family members are characteristically assembled with N-terminal TRPM homology regions (MHRs) and a C-terminal coiled-coil domain. This depolarizing modulation of cellular Ca^{2+} entry is important for cellular responses such as neuronal bursting activity, cardiac rhythm and the immune response. The The cryo-EM structure was determined for the most widespread Ca^{2+}-activated, non-selective (CAN) channel, human TRPM4, bound to both the agonist Ca^{2+} and the modulating V_{10} (PDB code 5WP6). The V_{10} was formed from a solution of 50 mM Na_3VO_4 adjusted to pH 2.0 from which 1 mM V_{10} and 5 mM calcium chloride was mixed with purified TRPM4 for a few hours before cryo-EM experiment. The cryo-EM structure of a human TRPM4 channel shown in Fig. 9A consists of a protein complex with Ca^{2+} and several V_{10} [126]. The Ca^{2+} ions are necessary for formation of the crystals although the density for the Ca^{2+} was not discernible, the patch-clamp recorded data showed Ca^{2+} activation that can be blocked by either flufenamic acid or ATP^{4-} consistent with the Ca^{2+} being agonist and associated with the active site. The global view of TRPM4 in Fig. 9A shows eight V_{10} moieties, four for each surface and internal characterized binding mode. Enlarged views of the two unique V_{10}'s binding modes are shown in Fig. 9B and Fig. 9C and show the high density of positively-charged residues surrounding each V_{10}. The V_{10} at the surface sites are characterized by the interaction of four Arg, two Ser, two Lys and one Gln side chain (Fig. 9B). The internally stabilized V_{10} is supported by three Arg, one Ser and one His side chain (Fig. 9C).

The crystal structure of the human cell cycle protein CksHs1 with kinase domain was shown to bind V_7 species, see Fig. 10 (PDB code 1DKT). However, as the authors described in the manuscript, they believed that the V-cluster in the protein was a V_{10} cluster with three disordered vanadates [113]. This protein is involved in cell-cycle progression, which is largely regulated up or down by the activity of cyclin-dependent kinases (Cdks) [127]. The Cdks act by phosphorylation and several Cdks have cell-cycle functions in eukaryotic species. Two human gene homologs, CksHs1 and CksHs2, have been cloned and found to functionally substitute for CKS1 in *S. cerevisiae* [128]. Both phosphate and vanadate bound to CksHs1 provided information on CksHs1-ligand interactions. The vanadate binds tightly to Cks and was successfully used for crystallizing CksHs1 [113]. Two phosphate-binding sites are located near the dimer interface within a crevice formed by the dimer association (Fig. 10).

CksHs1 crystallizes as a dimer with phosphate, tungstate [113] or vanadate. However, since vanadate oligomerizes and forms V_{10} in aqueous solution at acidic pH and V_{10} interacts with an activated receptor tyrosine kinase, it is possible that a cluster would be asso-

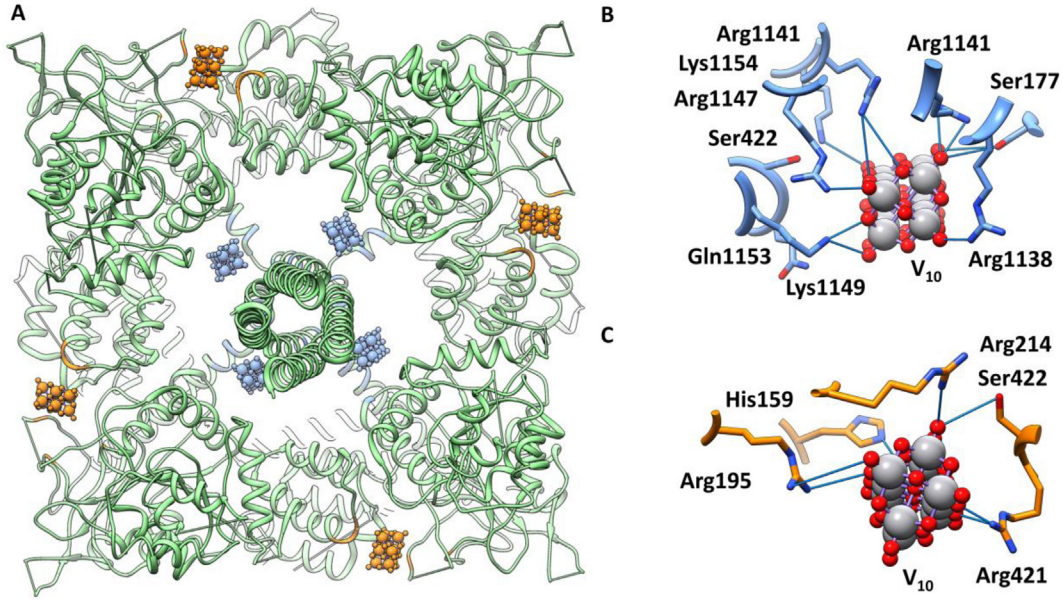

Fig. 9. Structure of the human TRPM4 (PDB code 5WP6) [126] channel shown in the complex with Ca^{2+} and V_{10}. A) global view; B) and C) close-up views of the two different binding modes of V_{10} with B) being the bound at the kink of the C-terminal helix (blue in A) and C) exposed at the interface of the N-terminal TRPM homology domain between the two adjacent subunits (orange in A). (For interpretation of the references to color in this figure legend, the reader is referred to the web version of this article.)

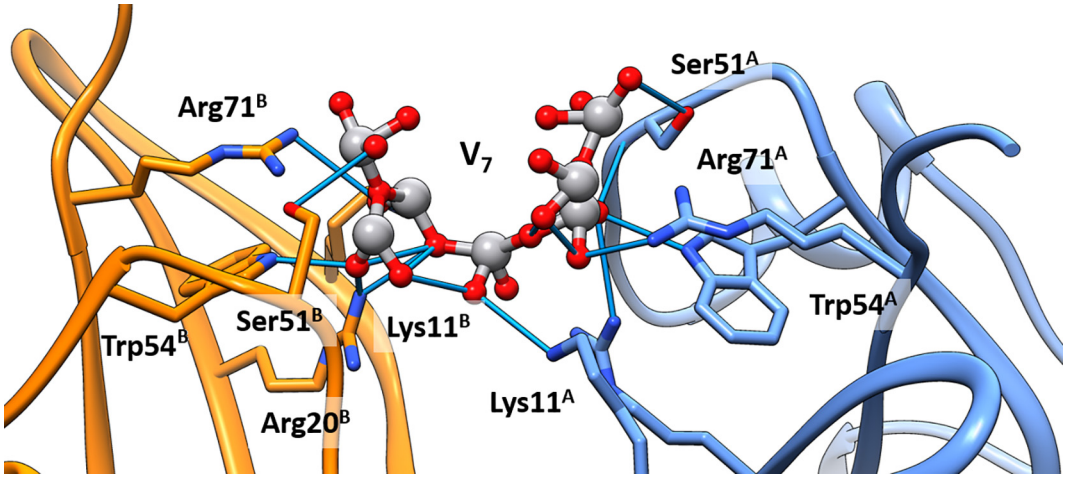

Fig. 10. Structure of human CksHs1 dimer (PDB code 1DKT) of the bound V_7 representing a partial V_{10}-cluster [113]. The authors assigned the protein complex to a Protein-V_{10} complex. Three disordered vanadate molecules would complete the putative V_{10} cluster, which on the basis of the electron density in the PDB is shown as V_7 [113]. H-bond contacts are depicted with blue lines. (For interpretation of the references to color in this figure legend, the reader is referred to the web version of this article.)

ciated with CksHs1. The authors noted a large positive region of electron density in their model, indeed larger than what is predictable for a mononuclear and even simple oligomeric species, which the authors presumed to be "metavanadate" given their crystallization conditions. As seen in the structure shown in Fig. 10, the observed electron density was modeled with seven V-atoms as a V_7. Because V_7 is not commonly observed in aqueous solution [41], the presence of a V_7 in a protein complex would represent the report of a new oxidovanadate species. Therefore, we considered the possibility that the V_7 structure would be more accurately described as another POV, as described below.

In this highly symmetric (D_3) structure, a region of high electron density sits along the symmetry axis and this was formulated as $\{V_7O_{19}\}$ in the deposition for 1DKT in the PDB [113]. Unfortunately, distances between V and O centers and atom arrangements leading to the suggested coordination geometries are inconsistent with the formulation of a V_7 structure. One possible interpretation, suggested by the authors, is that this POV is more likely to be V_{10} anion for which all the V-atoms are not fully occupied in the crystal structure. This interpretation is supported by the fact that the symmetry does not allow an asymmetric non-branching V_7 as formulated in the deposited structure and thus casting serious doubt on the interpretation of a novel V_7 species. Unlike in entry 3GQI [121], where the authors chose to use idealized coordinates and parameters to model the V_{10} in the structure, in the 1DKT it was assumed that the actual species is V_{10} with some electron density missing. The missing electron density has likely been modeled as solvent water and thus the authors labeled the rest of the V_{10} molecule as a V_7 moiety to rationalize the diffraction data. In summary, this report does not support a new V_7-protein complex, but an imperfect V_{10}-protein adduct missing some of the electron density needed to account for a complete V_{10} anion.

An alternative interpretation considers that the 1DKT structure, like 2D1G [114], contains more than one binding site for oxi-

dovanadates and, as such, could contain smaller species bound in addition to the postulated V_7/V_{10}. The smaller species bind in a shallow surface groove in positions occupied by phosphates in the corresponding phosphate-containing crystal structure. The V_7/V_{10} species appears to form hydrogen bonds with Lys, two Arg, and a backbone nitrogen of Ser in the modeling. Given the presence of smaller oxidovanadates in the structure, it is possible that the alternative interpretation of the V_7 is representing at least in part a mixture of smaller, disordered bound oxidovanadates with average electron density corresponding to a V_7.

Although only six proteins were found to bind V_{10}, from the protein descriptions above some common patterns do emerge. There are fundamentally two types of binding sites: i) *surface binding*, where V_{10} binds non-specifically to the surface of the protein; and ii) internal binding, where V_{10} binds within a specific pocket into the three-dimensional structure of the protein. In several cases of surface binding, the V_{10} is bound to the protein along with a simple vanadate, V_1. In each of these cases the V_{10} binding involves positive "patches" of the protein; the negatively charged POVs electrostatically interact with multiple positively charged side chains. In the larger V_{10}, there are more of these weak electrostatic interactions than in the case of V_1, making the surface binding relatively stronger. In two of the cases, although they are still relatively close to the protein surface, the side chains of the protein's amino acids wrap around the V_{10} anion, somehow creating a specific solvent excluded pocket. In these internal binding cases, the anion is associated more specifically and solidifies the interactions between the protein and the large V_{10}. In the following section, we will describe interactions with smaller POV anions.

3.1.3. V-protein complexes: $V_2/V_3/V_4/V_7$-protein adducts

In addition to V_{10}, there are several smaller POVs including V_2, V_3, V_4 (Fig. 1) and a V_7 that have been reported to form complexes with various proteins and have been investigated by X-ray diffraction methods. One of the first characterized structures of vanadate oligomers bound to proteins was the *E. coli* co-factor dependent phosphoglycerate mutase (dPGM) and the structure with a linear V_4 (Fig. 1F) bound has been determined at a 1.3 Å resolution, PDB code 1E59 [129] (Fig. 11A).

The dPGM enzyme is a structural homolog of rat prostatic acid phosphatase from *Rattus norvegicus* and catalyzes the reaction of 3-phosphoglycerate (3-PG) to form 2-phosphoglycerate (2-PG). The mechanism goes through the phosphoryl transfer to form 2,3-bisphosphoglycerate (2,3-BPG) and a dephosphorylated dPGM intermediate. This X-ray structural determination of dPGM shows a linear V_4 bound in the active site [129] (Fig. 11B). This structure remains the only reported case of binding of the linear tetrameric POV to a protein. The studies with vanadate provided insight into the mechanism of this reaction.

In neutral solutions, a cyclic tetrameric oxidovanadate $[V_4O_{12}]^{4-}$ (Fig. 1E) is stable, while a linear oxidovanadate $[V_4O_{13}]^{6-}$ (Fig. 1F) has been reported up to pH 9.0 [130]. The authors, reporting the V_4-dPGM structure, characterize the binding site of dPGM as basic, which is consistent with the interaction and stabilization of the linear oxidovanadate over the cyclic V_4 generally stable in aqueous solution, and observed in structures with PDB codes 1UZI and 1L7V [131,132] (Fig. 12). The structure of the V_4-dPGM shows the two internal V-atoms (V_2 and V_3) well defined by the electron densities, whereas the two terminal V-atoms are disordered and modelled with only half occupancy. Thus, the structure may be a disordered V_2 or V_3 which are present in aqueous solution [130] and which have been observed in 1H2F, Fig. 13 [133], and 3F9B [134], where POVs bind to *Bacillus stearothermophilus* phosphatase PhoE and *Yersinia* protein-tyrosine phosphatase YopH, respectively. The highly charged binding site of dPGM forms a strong V-protein complex replacing the sulfate binding. This protein hence illustrates the versatility of the interactions of oxidovanadates with enzymes formed from solutions containing different V-species including V-Tris adducts (aqueous solutions of vanadate in Tris and other buffers will form V-buffer complexes as described previously in detail [51,135,136], however additional complexes in a crystallization medium may be important to generate the envi-

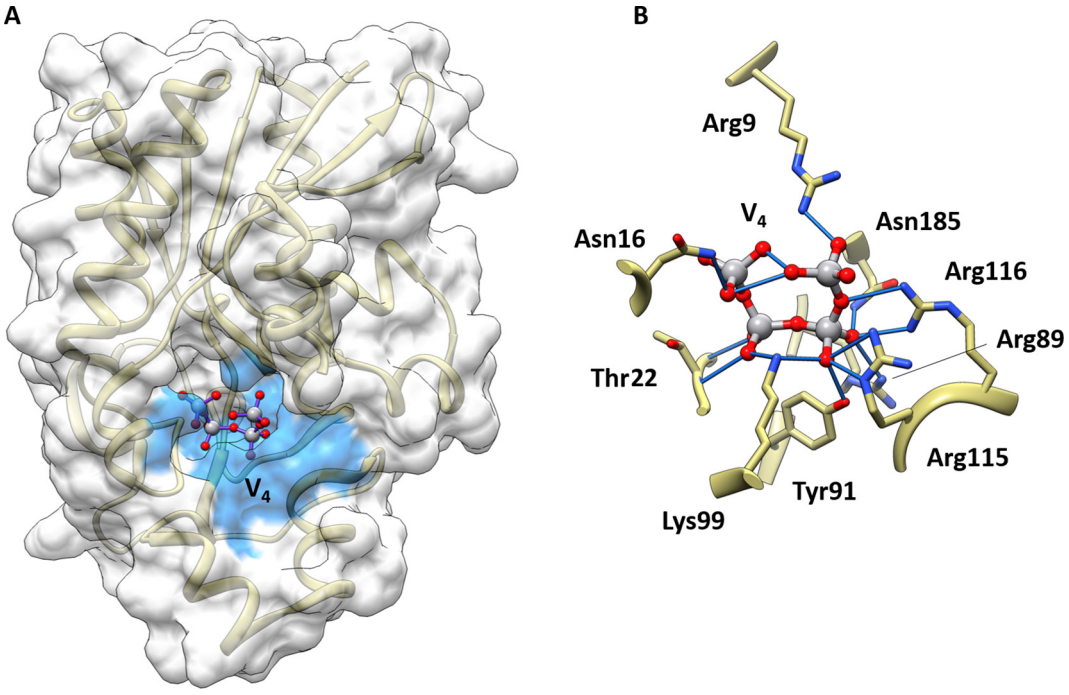

Fig. 11. The structure of linear V_4 bound to dPGM (PDB code 1E59). (A) Global view of the enzyme with V_4 in its active site; (B) close view of the H-bond network showing amino acid partners with O-atoms on the linear V_4 oxidovanadate.

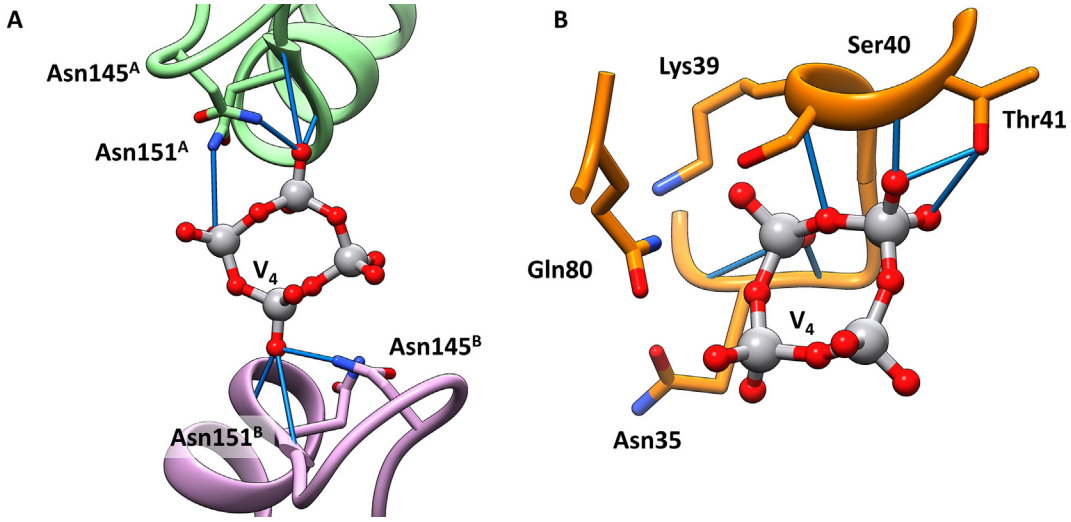

Fig. 12. Structure of the binding mode of cyclic V_4 toward: A) C3 exoenzyme for *Clostridium botulinum*, 1UZI; B) *E. coli* BtuCD protein, (PDB code 1L7V). H-bond contacts with electrostatics of V_4 the enzymes are depicted with blue lines [131,132]. (For interpretation of the references to color in this figure legend, the reader is referred to the web version of this article.)

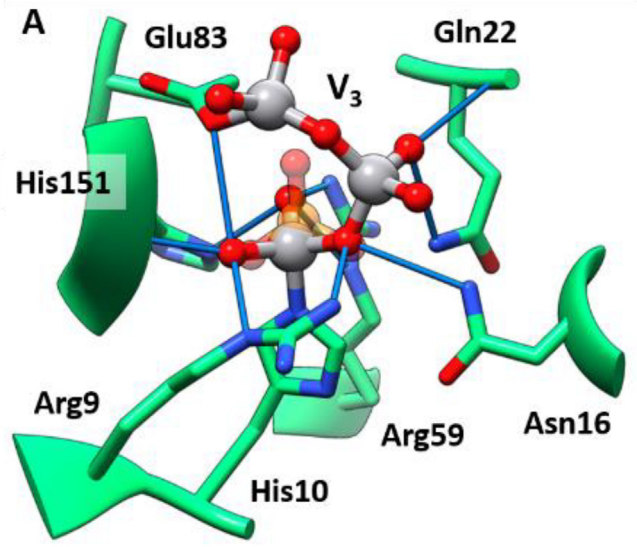

Fig. 13. Structure of the V_3 binding to the active site of phosphatase PhoE (PDB code 1H2F) along with the superposition of the native phosphate [133]. H-bond contacts are depicted with blue lines. (For interpretation of the references to color in this figure legend, the reader is referred to the web version of this article.)

ronment that allows a particular crystal to form). The linear V_4 is bound to dPGM in place of the four sulfate groups found in native dPGM structures, stabilized by an elaborate H-bond network, although the two internal V-atoms or sulfate groups are held tighter than the two terminal groups, Fig. 11B.

The two reported structures containing cyclic V_4-protein interactions are those of the C3 exoenzyme for *Clostridium botulinum*, (C3bot1, PDB code 1UZI), Fig. 12A [131], and *E. coli* BtuCD protein (PDB code 1L7V), Fig. 12B [132]. In C3bot1, the cyclic V_4 interacts loosely with the exoenzyme displaying contacts with asparagine side chains and the protein backbone (Fig. 12A). The binding site is found between biological assemblies holding together adjacent symmetry-equivalent domains. It is interesting that vanadate (V_1) similarly serves to bring together adjacent symmetry-equivalent domains at both ends of the assembly. Vanadate here thus serves as electrostatic "glue" to hold together the adjacent symmetry-equivalent domains. Similarly, the holding together of adjacent biological domains has been observed for other anisotropic POMs including the tellurium-centered Anderson polyoxidotungstate (TEW, $[TeW_6O_{24}]^{6-}$), which is now used as an effective technique to promote protein crystallization [137–141].

In the *E. coli* BtuCD protein, an ABC transporter involved in B12 uptake [132], the cyclic V_4 unit has more interactions than in C3bot1 as shown in Fig. 12B. Specifically, contacts with a threonine side chain and a long interaction with a glutamine from a neighboring chain are formed, but most are with protein backbone in a helical portion of the structure.

The complex of V_3 with *Bacillus stearothermophilus* phosphatase (PhoE) [133], a member of the cofactor-dependent phosphoglycerate mutase superfamily, has been characterized by X-ray crystallography (PDB code 1H2F) [133]. The V_3 is coordinated both to catalytic residues His10 and Glu83 that are part of an elaborate H-bonding network (Fig. 13). The V_3-PhoE complex was prepared through soaking of the PhoE-phosphate crystals prepared in 30.0% ethylene glycol, 25.0 mM AMP, and 55.0 mM sodium cacodylate buffer at pH 4.5 to which a solution of 50 mM NH_4VO_3, 30% ethylene glycol, 20 mM sodium acetate at pH 5.0 was added [133]. Because this mixture is incubated for three days, it is likely that the solution under those conditions contains V_{10} (Fig. 2), as well as a previously characterized complex with ethylene glycol [142], and yet the crystal formed containing the less stable V_3 anion, perhaps because of the size constraints of the binding site. The image in Fig. 13 shows that V_3 replaces the phosphate, forming an extensive H-bonding network in the V_3-PhoE complex. Hence the V_3-PhoE adduct is significantly different than the dPGM structure containing V_4 [129], where V_4 was found to form a strong complex replacing the four sulfate groups present in the native enzyme (Fig. 11). The association of V_3 with the PhoE protein is the only reported case so far involving V_3, with its unique availability of apoenzyme, product affinity, and phosphorylated intermediate structures. It seems likely that similar affinities will apply to other dPGM superfamily members. Indeed, modeling with adding V_3 into *E. coli* uridine phosphorylase was carried out and provided mechanistic details of this enzyme [117]. These observations are important because active, non-phosphorylated dPGM and inactive F26BPase structures as well as several other potential members of this superfamily of proteins have been identified in pathogenic organisms such as *Streptococci*, *Listeria*, *Staphylococcus aureus* and *Bacillus anthracis* [134].

A heptamer (V_7) was indicated in a deposited structure of *E. coli* uridine phosphorylase, PDB code 1RXS [117]. As mentioned above for the human cell cycle protein CksHs1 with PDB code 1DKT, a V_7 would represent a new species and was considered in detail by Arvai *et al.* [113] and now by us in preparation of this manuscript. Both Arvai *et al.* and us assigned the observed cluster to a V_{10} with missing electron density, even if Arvai *et al.* deposited the coordinates for the V_7 in PDB with code 1DKT. In the case of the structure of *E. coli* uridine phosphorylase, with PDB code 1RXS, electron density of a V-cluster assigned by Caradoc-Davies *et al.* [117] to the V_7 anion is found, even if no discussion was provided in the publication other than vanadate was used in the crystallization and for the solution of the structure. Given that the V_7 in 1DKT was just an electron density model, not an actual proposal of a structure, we favor an interpretation for the vanadium species to be something other than V_7. However, since there are not enough details provided by Caradoc-Davies *et al.* [117], we cannot deduce whether this structure contains one or more of the smaller oxidovanadates or a V_{10}.

In addition to the V_3, V_4, and V_7 POV interactions with proteins, a few reports have described V_2-protein adducts [94]. The systems range from simply pyrophosphate analogs to a diamond core complex associated with the vanadium. One very interesting case is one of the vanadate-*Yersinia* phosphatases structures (PDB code 3F9B) [134], where the dimer that is associated with the structure contains vanadium with two different coordination geometries [134]. The vanadium associated with the protein has a five-coordinate trigonal bipyramidal geometry whereas the free, terminal vanadium is four-coordinate and tetrahedral and is exemplary of the influence the protein can have on the coordination environment of oxidometalates [94].

In this section, we have discussed the binding of POVs described as a V_2, V_3, V_4, and a putative V_7. These former three structures show a greater diversity than those reported for the binding of V_{10}, whereas the reports with V_7 are likely a result of a decomposed or disordered POV or an incomplete electron density. In all these studies, complementarity between protein and POVs is high for crystals to form and in some cases so high that even less-stable POVs can give rise to tight V-protein adducts.

3.2. POVs and muscle contraction

According to Tables 1 and 2, V_{10} interacts with several proteins including those involved in the mechanism and regulation of muscle contraction – myosin, actin and Ca^{2+}-ATPase [39,49,56]. It is common for V_{10} to interact with ATP binding proteins, but it also interacts and inhibits other enzymes such as membrane channels and RNA ribonucleases (Tables 1 and 2). Sarcoplasmic reticulum (SR) calcium pump has proven to be an excellent model to study toxicology effects of POVs on P-type ATPases, such as the Na^+,K^+-ATPase and Ca^{2+}-ATPase. These ion pumps are involved in essential ions homeostasis, such as Na^+, K^+ and Ca^{2+}, therefore regulating several key cellular processes. Although Table 1 represents only data since 1989, it has been known since 1982 that V_{10} interacts with SR Ca^{2+}-ATPase [84,143]. Thus, V_{10} has a higher inhibition capacity compared to V_1 alone and different abilities to induce changes in the structure and function of the enzyme, as described, for instance, for myosin, actin and calcium pump [39,49,56,99,144]. Recently, another POV, $Cs_{5.6}H_{3.4}PV_{14}O_{42}{\cdot}12H_2O$ (PV_{14}, Fig. 1I), was described to inhibit P-type ATPases, being particularly more potent than V_{10} (IC_{50} = 15 μM) in the inhibition of the Ca^{2+}-ATPase (IC_{50} = 0.6 μM) [57].

Regarding of actomyosin ATPase inhibition by V_{10}, the first studies were described in 1988, using flow microcalorimetry [145]. In 2004 [49], it was reported that such an inhibition implies a myosin binding site different from ATP site, and that V_{10} inhibition is non-competitive. These studies clearly demonstrated that, unlike V_1, V_{10} species can strongly inhibit the myosin actin-stimulated ATPase activity with an IC_{50} of 6.1 μM for V_{10}, whereas no inhibitory effects were detected for V_1 up to 150 μM [49]. It was proposed, combining molecular docking simulations with kinetic studies, that V_{10} interacts with the phosphate-binding domains in the vicinity of the designated "back-door" binding site (Fig. 14) [49,104]. Thus, an intermediate myosin·MgATP·V_{10} complex is formed, which inhibits the myosin-actin interactions associated with ATP hydrolysis by actomyosin, and the blocking of the muscle contraction process most likely occurs in a pre-hydrolysis state [49,99,104]. Note that the walker A motif (corresponding to the P-loop in myosin), as well as the ABC (ATP-binding cassette) ATPases, were also described as an anion-binding domain that can interact with this POV with high affinity [92,104].

In contrast to the examples described above, for a long time there was no available information on the molecular interaction of V_{10} with actin, another major protein of the contractile system of muscle cells. The first report describing the interaction between V_{10} and actin was published in 2006, suggested that G-actin, the globular monomeric form of actin, stabilizes decavanadate species by increasing the half-life time of decomposition from 5 to 27 h [39]. V_{10} inhibits the rate of G-actin polymerization into F-actin (polymerized form of actin), with an IC_{50} of 17 μM [39], suggesting that it would affect cytoskeleton structures responsible for many processes of relevant biological significance. These studies were further explored and described protein cysteine oxidation together with vanadate reduction upon V_{10} incubation with actin [63]. Additionally, it was also shown that V_{10} binding induces an opening of the G-actin cleft. V_{10} was able to oxidize Cys374 in F-actin and one of the protein core cysteine residues, presumably Cys272 [63,64]. In fact, the interaction of V_{10} with G-actin results in a vanadate(V) reduction to oxidovanadium(IV) ion. Moreover, in the presence of ATP in the medium assay, the reduction of V^V to V^{IV} is prevented and all five G-actin cysteine residues remain in their reduced form [63,109].

In 2021, molecular dynamics and docking studies were described in order to attain an understanding at molecular level of the V_{10}–G-actin interaction, rationalizing the results obtained during the last 15 years by several spectroscopic techniques [64]. Four binding sites of V_{10} were identified, named α, β, γ, and δ, the site α being the catalytic nucleotide site located in the cleft of the enzyme at the interface of the subdomains II and IV. The site α is stabilized by H-bonds with Gln59, Arg62, Tyr69, Thr204, Arg207, and Arg211 residues. The site α is more stable than site β by more than 20 kcal·mol^{-1} and much more for sites γ and δ [64].

A slight opening of the nucleotide binding site α is predicted after the interaction with V_{10} which varies the cleft opening (defined as the $C(\alpha)_{Lys67}$-$C(\alpha)_{Val339}$-$C(\alpha)_{Thr203}$ angle) from 28.6° in the apo form to 35.6° in the adduct with V_{10}, with a rearrangement of the H-bonds. The behavior of V_{10} was compared with the bulkier isostructural polyoxidoniobate (PONb) Nb_{10} (volume of 594.3 Å^3 vs. 520.6 Å^3 of V_{10}) which is more stable at the site β [64].

ATP is found at the site α, the enzymatic cleft of G-actin, and this ATP binding is more favorable by 14.1 kcal mol^{-1} than V_{10}. MD studies indicated that the presence of ATP hinders the V_{10} binding, which is forced to reach the site β. Notably, the competition is less important for Nb_{10} because this POM shows a higher affinity for site β than for site α, suggesting that both POVs and PONbs could contemporaneously bind to G-actin, making their action synergistic, a finding that should be possible for other POMs-protein systems (Fig. 15) [64].

Finally, in the study mentioned above, it was demonstrated that the binding mode of $V^{IV}O^{2+}$ ion, formed upon the V_{10} reduction by Cys residues, is in the catalytic site α with (His161, Asp154) coor-

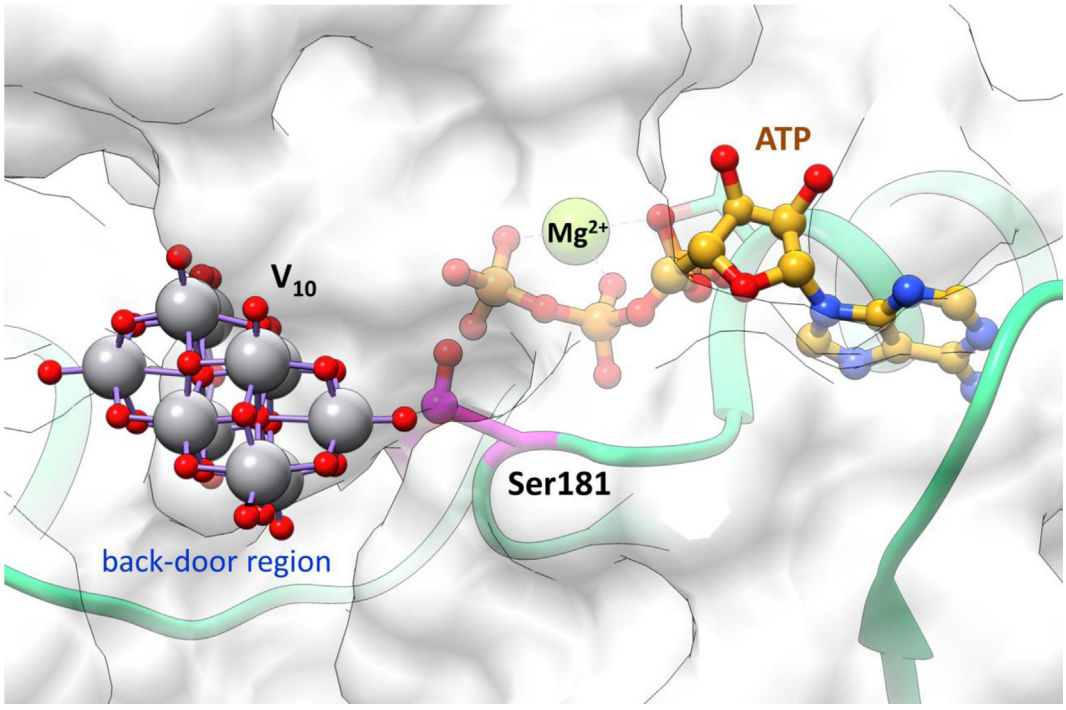

Fig. 14. Docking solution of V_{10} interacting with myosin at the phosphate-binding domain, in the vicinity of the nominated "back-door" binding site (adapted from ref. [104]). Color code: V, grey, O, red. (For interpretation of the references to color in this figure legend, the reader is referred to the web version of this article.)

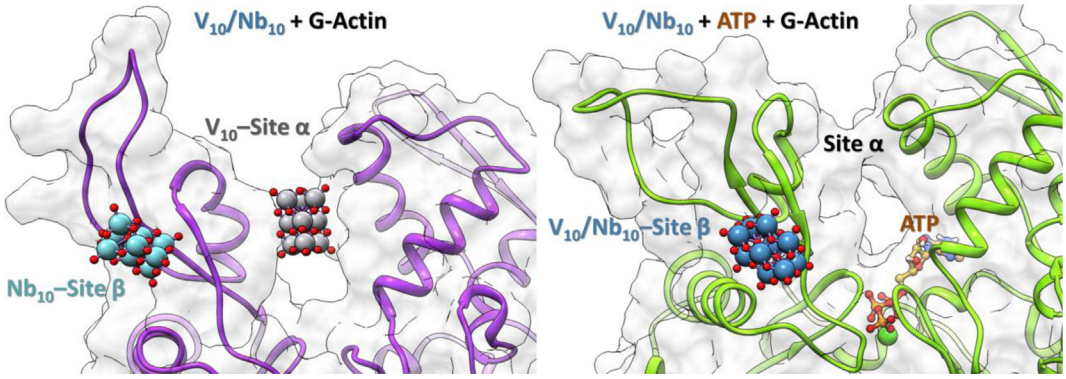

Fig. 15. V_{10}/Nb_{10} actin interactions predicted by molecular dynamics and docking studies (adapted from ref. [64]). Color code: V, grey; Nb, blue; O, red. (For interpretation of the references to color in this figure legend, the reader is referred to the web version of this article.)

dination; interestingly, this adduct overlaps significantly with the region where ATP is bound, accounting for the competition between V_{10} and $V^{IV}O^{2+}$ with ATP, observed by EPR spectroscopy [64].

3.3. POVs' interactions with serum proteins

After the administration of a POV, it may or may not reach the bloodstream intact, depending on the mode of administration [146]. The interaction of a POV with serum proteins is most likely to occur with intravenous administration or if the compound easily penetrates the cells membranes required to reach the blood, where POV would be associated with the serum fraction. In serum, a POV encounters several biomolecules and, in particular, proteins like human serum transferrin (HTf) and human serum albumin (HSA). Transferrins are a group of single-chain glycoproteins having 700 amino acids with a mass of ca. 80 kDa with a concentration in blood around 30 μM [147,148]. In human serum, HTf transports not only iron [149], but also other metal ions such as Bi, Al, Ru, Mn, Ni, and V in its three oxidation states stable in biological systems (+III, +IV, +V) [61,150]. Considering the iron amount in the two specific sites in the N- and C-terminal, the concentration of available sites for metal binding is ca. 34 μM [151]. HSA is the most abundant blood protein with a concentration around 640 μM [148] and transports, beside essential and toxic metal ions and their compounds [152], fatty acids and endogenous and exogenous ligands [153].

It was recently described that V_{10} interacts both with HSA and HTf, presumably through non-covalent binding (see section 3.1), but surprisingly $(2\text{-}hepH)_2[\{Co(H_2O)_5\}_2V_{10}O_{28}]\cdot 4H_2O$ ($V_{10}Co$, 2-*hep*H = 2-hydroxyethylpyridinium) exhibits high affinity toward transferrin but does not interact with albumin [43]. It was supposed that the Co^{II} centers coordinated to {VO} groups of V_{10} occupy the binding sites of V_{10}, blocking its interaction with the albumin protein [43]. In contrast, HTf shows interaction with $V_{10}Co$, but the reasons for this different behavior should be examined in detail at an experimental and computational level. The different behavior of $V_{10}Co$ was also shown by two model pro-

teins: in proteinase K, V_{10}Co interacts more strongly than thaumatin [43].

3.4. POVs and diabetes

According to the WHO, about 400 million individuals worldwide have diabetes, which can cause heart disease, stroke, kidney damage, and even death [154]. Insulin, which is produced by β-cells found in pancreatic islets, regulates the metabolism of carbohydrates. In 2021, it will be 100 years since insulin was discovered by Banting, Best and McLeod at the University of Toronto [28,155,156]. Vanadium has also long been associated with diabetes; in 1899, French scientists reported the blood glucose-lowering effect of vanadium [157]. However, it was only by 1979 that it was shown that vanadium salts exhibit insulin-enhancing effects, leading to a growing interest in vanadium compounds for the treatment of diabetes [158–160]. Since then, insulin-like effect of various vanadium compounds, mainly oxidovanadium(IV) sulfate and organic vanadates have been described [146]. One organic vanadium compound, bis(ethylmaltolato)oxidovanadium(IV), entered Phase I and II clinical trials [156]. However, vanadium coordination complexes are not the purpose of the present review, and the interested reader should address that elsewhere [158,161,162]. Therefore, the antidiabetic potential of POVs and vanadium-substituted POMs is described here.

Certain polyoxidometalates are known to have insulin-enhancing properties [163]. Also, some POVs, for instance V_{10}, have been shown to enhance glucose uptake in rat adipocytes [7]. Moreover, a hybrid decavanadate compound namely metformin (Metf) decavanadate, $(H_2Metf)_3V_{10}$, showed hypoglycemic and lipid-lowering effects in animal models of both insulin-dependent (type 1) and insulin-independent diabetes (type 2) [8] beyond those observed with metformin itself. The insulin-mimetic effect of benzylamine-decavanadate $(C_7H_{10}N)_6V_{10}$ was also studied [9]. As with $(H_2Metf)_3[V_{10}O_{28}]$, $(C_7H_{10}N)_6V_{10}$ stimulated glucose transport and normalized the lipid profile. Also recently, a second compound, $[DMAPH]_4(NH_4)_2V_{10}$ (DMAPH = 4-dimethylaminopyridinium), showed hypoglycemic and lipid-lowering effects [164].

The exact POVs mechanism remains unknown for both type 1 and 2 diabetes. However, the POVs insulin-enhancer effect might, among others, derive from V_{10} inhibition of protein tyrosinase phosphatase, an enzyme catalyzing the dephosphorylation of the insulin receptor, which turns off insulin signaling. It was also suggested that $(H_2Metf)_3V_{10}$ interferes with the mitochondrial electron transport chain, forcing lipid oxidation. In fact, V_{10} was previously described to target mitochondria strongly affecting oxygen consumption and mitochondria membrane depolarization [106], and to induce necrotic death in neonatal rat cardiomyocytes through mitochondrial membrane depolarization [165]. More recently, it was referred that a mixed POM containing vanadium, $K_{11}H[(VO)_3(SbW9O_{33})_2]$, which exerts hypoglycemic effects in streptozotocin-induced diabetic rats, shows hepatic protective properties and stimulation of insulin synthesis [166]. These findings clearly show that V-containing POMs are not only insulin-enhancers, as suggested before for other vanadium compounds, but also stimulate the insulin synthesis [146,167].

Besides hyperglycemia and hyperlipidemia, oxidative stress contributes to the pathogenesis of diabetes. Recently, the oxidative stress in multiple tissues of alloxan-induced diabetic rats (type 1 diabetes) and the effect of $(H_2Metf)_3V_{10}$ on this stress was evaluated [168]. It was described that $(H_2Metf)_3V_{10}$ reduced oxidative stress by positively affecting the nuclear factor erythroid 2-related factor 2 (NRF2), a transcription factor responsible for cellular antioxidants. Thus, POVs mediated activation of NRF2 induces the expression of reduced glutathione (GSH), superoxide dismutase (SOD), and catalase (CAT), restoring cellular antioxidants defenses.

POVs inhibition of α-glucosidase, which converts carbohydrates into glucose, is another strategy for the treatment of diabetes. About 10 mixed polyoxidomolybdates (POMos) containing vanadium have been described to exhibited inhibitory effects on α-glucosidase [169,170,171]. One of them, $H_6[PMo_9V_3O_{40}]$, exhibits higher activity (IC_{50}, 9.6 μM) than acarbose (IC_{50}, 38.2 μM), a clinically used antidiabetic drug and α-glucosidase inhibitor [172]. For comparison, higher potency POMs α-glucosidase inhibitors include $H_6[P_2Mo_{18}O_{62}]$ (IC_{50} = 0.17 μM) and $H_3[PMo_{12}O_{40}]$ (IC_{50} = 6.1 μM)

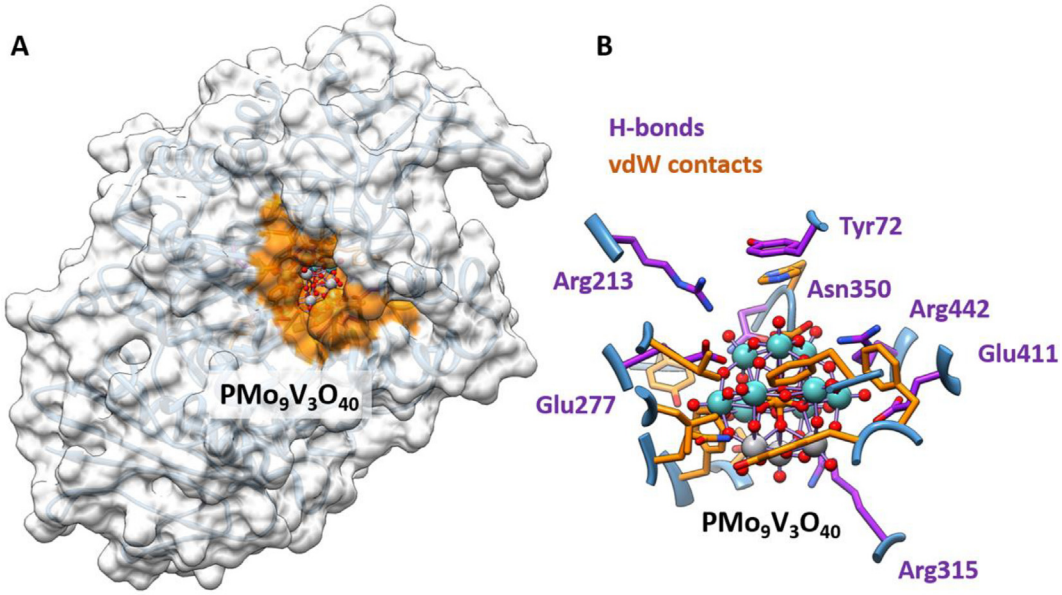

Fig. 16. Representation of the docking solution of $[PMo_9V_3O_{40}]^{6-}$ bound to α-glucosidase. A) global view of the enzyme with $[PMo_9V_3O_{40}]^{6-}$ in its active site; and (B) close view of the secondary interactions network. H-bond donors depicted in purple and vdW interactors in orange (His351, Thr306, Tyr347, Gln279, Tyr158, Asp352, Phe159, Phe178, Leu219, Val216, Phe303). Adapted from ref. [171]. (For interpretation of the references to color in this figure legend, the reader is referred to the web version of this article.)

[170,173]. For $H_6[PMo_9V_3O_{40}]$ the mixed type of inhibition was described, and the structure predicted from docking studies is shown in Fig. 16.

3.5. POVs and oxidative stress responses

As referred in the above section, the mode of action of POVs in diabetes might be due to, inter alia, direct or indirect changes in cellular oxidative responses. However, owing to the low stability of V_{10} under physiological conditions, it is expected that it dissociates into minor oxidovanadates namely V_1, V_2 and V_4, presumably involved in the biological effects observed. The detoxification mechanism proposed for vanadate involves bioreduction of vanadate to oxidovanadium(IV) by glutathione (GSH) [174]. Therefore, GSH is an important cellular antioxidant defense system and directly or indirectly regulates the levels of ROS [175,176]. On the other hand, in Fenton-like reactions vanadate is reduced to $V^{IV}O^{2+}$ with production of $OH^{\cdot}$ [177,178]. However, vanadium prooxidants effects are not the purpose of the review and the reader is referred elsewhere [146,167]. Since the beginning of the 21 century, the Aureliano research group has been performing POVs *in vivo* studies, mainly with V_{10}, in order to determine the contribution of V_{10} species to toxic effects observed in fish at room temperature where V_{10} stability is higher [40,55,179,180]. Following V_{10} *in vivo* administration, several oxidative stress parameters were ascertained in fish: reduced GSH content, overall rate of ROS production, lipid peroxidation, and antioxidant enzyme activities [40,55,179,180]. It was concluded that V_{10} clearly induces different and, in many times, opposite effects than the ones observed for vanadate [181,182]. For instance, upon V_{10} exposure, an increase in GSH content and ROS production was observed, as well as a decrease in mitochondrial antioxidant enzymes activities such as SOD and catalase activities, whereas opposite or no effects were observed for vanadate [40,55]. Therefore, it was suggested that POVs species exposure follows different pathways than vanadate for the generation of reactive oxygen species and that they interfere differently with some of the enzymes involved in antioxidant defenses in cells [182,183].

In summary, studies describing POVs, mainly V_{10} interactions with proteins (Fig. 17) include, among others: 1) proteins associated with diabetes such as phosphatases, tyrosine kinases and glucosidases; 2) membrane channels such as TRPM4 channels, ATP sensitive channels, porin VDAC modulator and P2X receptor; 3) muscle contraction proteins such as myosin and actin; 4) serum proteins, such as albumin and transferrin; 5) P-type ATPases such as Ca^{2+}-ATPase pumps; 6) mitochondria proteins such as complex

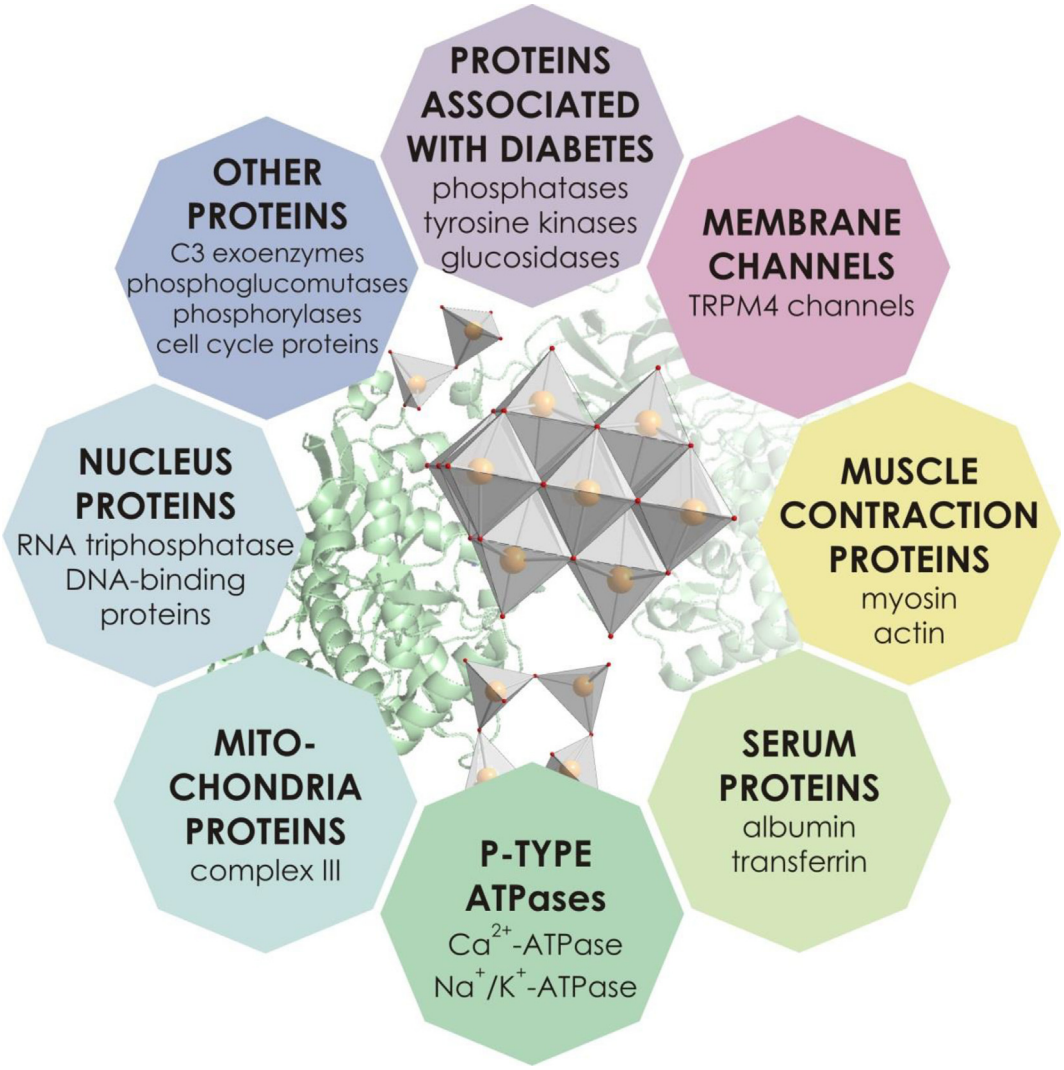

Fig. 17. Scheme of the described interactions of proteins with POVs such as V_2, V_4, and V_{10}. POVs' interactions include muscle contraction proteins, channels, receptors and ion pumps, mitochondria proteins, nucleus proteins, serum proteins as well as those associated with diabetes, among others.

III and 7) nucleus proteins, such as RNA triphosphatase and DNA-binding protein. Smaller POV proteins interactions include, among others: 8) phosphoglucomutases; C3 exoenzymes; cell cycle proteins and phosphorylases (Fig. 17).

4. Conclusions and perspectives

In summary, we have described from a qualitative and quantitative point of view information about the interaction of several POVs, particularly V_{10}, with several key cellular proteins including phosphatases, NTPDases, TRPM4 channel, tyrosine kinases, myosin actin, transferrin, albumin and glucosidases, among others. Considering the methods available to determine speciation and mode of actions, this subgroup of POMs is likely to receive much more interest in the near future as probes for enzymes and in biomedical applications. The application of POVs, being pure, POVs-based hybrids and/or nanomaterials containing POVs in various biological systems, is a rapidly growing branch of science.

The understanding of the POVs interactions with proteins remains the key step for elucidating the biomedical mechanism of action of these compounds, and in this review, we examined both the molecular interactions through reported POV-protein structures from X-ray crystallographic reports as well as studies characterizing these interactions using computational methods. In spite of the fact that simple vanadate salts are often used for the experimental treatment, the POVs can form under the conditions of the studies. In the reported cases, POVs seem to exert their cellular effects by interacting with the numerous proteins in the respiratory chain and the cytoskeleton, with the ionic transport systems, as well as with DNA, among others, and the molecular interactions are affecting structure and function.

Besides hydrogen bonds, electrostatic and van der Waals interactions contribute to POVs binding to proteins. The X-ray structures of V_{10}-proteins show that there are two groups of POV-protein interactions, those located at the surface or at the interior of the proteins. In both cases, the binding sites are characterized by complementary interactions of a positive patch on the protein surface where the V_{10} will form several H-bonds and electrostatic salt bridges. The positively charged residues include a variety of Lys, Arg, and His and in an organized manner complementary surrounding the V_{10} anion, strengthening the surface interaction. Of particular interest is the V_{10} myosin back-door interaction and also its reduction by actin that is prevented by the native ligand MgATP. In spite the low stability of POVs at physiological pH, the half-life of V_{10} is increased in serum, suggesting an interaction with proteins that can stabilize its structure. Some proteins, such as actin, improve 6-fold the stability of V_{10}.

Examples of less common POVs forming V-protein adducts were also summarized. These systems are very interesting in that these include interactions of vanadate with kinases, signaling molecules and phosphoglucomutases and phosphoglyceratemutases and the formation of V_2-protein, V_3-protein, V_4-protein, as well as V_1-protein adducts was demonstrated. However, there are two reported V_7-protein complexes, whose electronic density is often diffuse and does not lead to clear solutions. In one case the study was exhaustive and showed that the system is not likely to involve a new V_7 POV, but the results instead are better explained by V_{10} or a combination of smaller oxidovanadates.

A couple of POVs is actually binding the less stable linear V_3 and linear V_4, which are not observed in aqueous solution at pH 7. Interestingly, in these cases the POV-proteins interactions are sufficiently stable and the result is the formation of complexes between proteins and uncommon and less stable POVs present only in small amounts from the crystallization media. The reported V-protein complexes must bind the V-cluster very tightly and be stabilized by both primary and secondary non-covalent interactions.

POVs, especially modified V_{10}, showed promising antidiabetic effects in animal models of type 1 and 2 diabetes. However, other activities have recently been reported including antimicrobial activities. V_{10} and Pt and Mo mono-substituted V_{10} were found to inhibit growth of *Mycobacteria smegmatis* and/or *Mycobacteria tuberculosis*. Furthermore, the POVs were reported to initiate signaling and, in this case, it was not only V_{10} but also multivalent V_{14} and V_{15} POVs that were active.

In summary, this review demonstrates the quantity and quality of information now available characterizing the POVs' interaction with proteins and enzymes. Studies reported have used a range of methods to determine speciation and mode of actions. Undoubtedly, the POV subgroup of POMs is likely to receive much more interest in the near future given their ability to serve as probes for enzymes and their direct effects in biomedical applications. With so few POV-protein structures reported and the known ability of POMs to assist in crystallization, it is very likely that the number of reported POV-protein structures will increase. Moreover, we also predict that the future will show that a number of different hetero-POVs will be biologically active. Such an approach will allow for obtaining not only clusters with mixed metal ions in addition to vanadium atoms, but also multivalent POVs, i.e. containing both V^{IV} and V^{V}. As was illustrated in a few available studies, the structural framework from the vanadium will be maintained but substitutions will allow for more diverse redox chemistry and biological activities. The future is indeed bright for POVs.

Declaration of Competing Interest

The authors declare that they have no known competing financial interests or personal relationships that could have appeared to influence the work reported in this paper.

Acknowledgments

This research was funded by FCT – Foundation for Science and Technology through project UIDB/04326/2020 (M.A.); Regione Autonoma della Sardegna through the grant RASSR79857 and Fondazione di Sardegna through the project FdS2017Garribba (G.S. and E.G.); Spanish MICINN' Juan de la Cierva program, FJC2019-039135-I (G.S.); the Austrian Science Fund (FWF): P33927 (N.G.); P33089 (A.R.); the University of Vienna (N.G. and A.R.); Illinois State University (C.C.M.) and Colorado State University (D.C.C.).

References

[1] H. Stephan, M. Kubeil, F. Emmerling, C.E. Müller, Polyoxometalates as versatile enzyme inhibitors, Eur. J. Inorg. Chem. 2013 (2013) 1585–1594, https://doi.org/10.1002/ejic.201201224.

[2] T.L. Turner, V.H. Nguyen, C.C. McLauchlan, Z. Dymon, B.M. Dorsey, J.D. Hooker, M.A. Jones, Inhibitory effects of decavanadate on several enzymes and *Leishmania tarentolae In Vitro*, J. Inorg. Biochem. 108 (2012) 96–104, https://doi.org/10.1016/j.jinorgbio.2011.09.009.

[3] S.-Y. Lee, A. Fiene, W. Li, T. Hanck, K.A. Brylev, V.E. Fedorov, J. Lecka, A. Haider, H.-J. Pietzsch, H. Zimmermann, J. Sévigny, U. Kortz, H. Stephan, C.E. Müller, Polyoxometalates - potent and selective ecto-nucleotidase inhibitors, Biochem. Pharmacol. 93 (2) (2015) 171–181, https://doi.org/10.1016/j.bcp.2014.11.002.

[4] S.H. Saeed, R. Al-Oweini, A. Haider, U. Kortz, J. Iqbal, Cytotoxicity and enzyme inhibition studies of polyoxometalates and their chitosan nanoassemblies, Toxicol. Reports 1 (2014) 341–352, https://doi.org/10.1016/j.toxrep.2014.06.001.

[5] D.C. Crans, Enzyme interactions with labile oxovanadates and other polyoxometalates, Comm. Inorg. Chem. 16 (1–2) (1994) 35–76, https://doi.org/10.1080/02603599408035851.

[6] Ş. Bâlici, S. Şuşman, D. Rusu, G.Z. Nicula, O. Soriţău, M. Rusu, A.S. Biris, H. Matei, Differentiation of stem cells into insulin-producing cells under the

influence of nanostructural polyoxometalates, J. Appl. Toxicol. 36 (3) (2016) 373–384, https://doi.org/10.1002/jat.3218.
[7] M.J. Pereira, E. Carvalho, J.W. Eriksson, D.C. Crans, M. Aureliano, Effects of decavanadate and insulin enhancing vanadium compounds on glucose uptake in isolated rat adipocytes, J. Inorg. Biochem. 103 (12) (2009) 1687–1692, https://doi.org/10.1016/j.jinorgbio.2009.09.015.
[8] S. Treviño, E. Sánchez-Lara, V.E. Sarmiento-Ortega, I. Sánchez-Lombardo, J.Á. Flores-Hernández, A. Pérez-Benítez, E. Brambila-Colombres, E. González-Vergara, Hypoglycemic, lipid-lowering and metabolic regulation activities of metforminium decavanadate $(H_2Metf)_3V_{10}O_{28}{\cdot}8H_2O$ using hypercaloric-induced carbohydrate and lipid deregulation in Wistar rats as biological model, J. Inorg. Biochem. 147 (2015) 85–92, https://doi.org/10.1016/j.jinorgbio.2015.04.002.
[9] S. García-Vicente, F. Yraola, L. Marti, E. González-Muñoz, M.J. García-Barrado, C. Cantó, A. Abella, S. Bour, R. Artuch, C. Sierra, N. Brandi, C. Carpéné, J. Moratinos, M. Camps, M. Palacín, X. Testar, A. Gumà, F. Albericio, M. Royo, A. Mian, A. Zorzano, Oral insulin-mimetic compounds that act independently of insulin, Diabetes 56 (2) (2007) 486–493, https://doi.org/10.2337/db06-0269.
[10] J. Zhao, K. Li, K. Wan, T. Sun, N. Zheng, F. Zhu, J. Ma, J. Jiao, T. Li, J. Ni, X. Shi, H. Wang, Q. Peng, J. Ai, W. Xu, S. Liu, Organoplatinum-substituted polyoxometalate inhibits β-amyloid aggregation for Alzheimer's therapy, Angew. Chem. Int. Ed. 58 (2019) 18032–18039, https://doi.org/10.1002/anie.201910521.
[11] J. Iqbal, M. Barsukova-Stuckart, M. Ibrahim, S.U. Ali, A.A. Khan, U. Kortz, Polyoxometalates as potent inhibitors for acetyl and butyrylcholinesterases and as potential drugs for the treatment of Alzheimer's disease, Med. Chem. Res. 22 (3) (2013) 1224–1228, https://doi.org/10.1007/s00044-012-0125-8.
[12] Y. Hayashi, Hetero and lacunary polyoxovanadate chemistry: Synthesis, reactivity and structural aspects, Coord. Chem. Rev. 255 (2011) 2270–2280, https://doi.org/10.1016/j.ccr.2011.02.013.
[13] A. Bijelic, M. Aureliano, A. Rompel, Polyoxometalates as potential next-generation metallodrugs in the combat against cancer, Angew. Chem., Int. Ed. 58 (2019) 2980–2999, http://doi.org/10.1002/anie.201803868 (Angew. Chem. 131 (2019) 3008–3029, http://doi.org/10.1002/ange.201803868).
[14] A. Bijelic, M. Aureliano, A. Rompel, The antibacterial activity of polyoxometalates: structures, antibiotic effects and future perspectives, Chem. Commun. 54 (2018) 1153–1169, https://doi.org/10.1039/C7CC07549A.
[15] A. Bijelic, A. Rompel, The use of polyoxometalates in protein crystallography – an attempt to widen a well-known bottleneck, Coord. Chem. Rev. 299 (2015) 22–38, https://doi.org/10.1016/j.ccr.2015.03.018.
[16] A. Bijelic, A. Rompel, Polyoxometalates – more than a phasing tool in protein crystallography, ChemTexts 4 (2018) 10, https://doi.org/10.1007/s40828-018-0064-1.
[17] J.M. Missina, L.B.P. Leme, K. Postal, F.S. Santana, D.L. Hughes, L. de Sá, R.R. Ribeiro, G.G. Nunes, Accessing decavanadate chemistry with tris (hydroxymethyl)aminomethane, and evaluation of methylene blue bleaching, Polyhedron 180 (2020), https://doi.org/10.1016/j.poly.2020.114414 114414.
[18] Y.-F. Song, R. Tsunashima, Recent advances on polyoxometalate-based molecular and composite materials, Chem. Soc. Rev. 41 (2012) 7384–7402, https://doi.org/10.1039/C2CS35143A.
[19] S.-M. Wang, J. Hwang, E. Kim, Polyoxometalates as promising materials for electrochromic devices, J. Mat. Chem. C 7 (26) (2019) 7828–7850, https://doi.org/10.1039/C9TC01722D.
[20] S.-S. Wang, G.-Y. Yang, Recent advances in polyoxometalate-catalyzed reactions, Chem. Rev. 115 (11) (2015) 4893–4962, https://doi.org/10.1021/cr500390v.
[21] S.Y. Lai, K.H. Ng, C.K. Cheng, H. Nur, M. Nurhadi, M. Arumugam, Photocatalytic remediation of organic waste over Keggin-based polyoxometalate materials: a review, Chemosphere 263 (2021) 128244, https://doi.org/10.1016/j.chemosphere.2020.128244.
[22] M.B. Čolović, M. Lacković, J. Lalatović, A.S. Mougharbel, U. Kortz, D.Z. Krstić, Polyoxometalates in biomedicine: update and overview, Curr. Med. Chem. 27 (3) (2020) 362–379, https://doi.org/10.2174/0929867326666190827153532.
[23] J.T. Rhule, C.L. Hill, D.A. Judd, R.F. Schinazi, Polyoxometalates in medicine, Chem. Rev. 98 (1) (1998) 327–358, https://doi.org/10.1021/cr960396q.
[24] M. Aureliano, N.I. Gumerova, G. Sciortino, E. Garribba, A. Rompel, D.C. Crans, Polyoxovanadates with emerging biomedical activities, Coord. Chem. Rev. 447 (2021), https://doi.org/10.1016/j.ccr.2021.214143 214143.
[25] M.T. Pope, A. Müller, Polyoxometalate chemistry: an old field with new dimensions in several disciplines, Angew. Chem., Int. Ed. 30 (1991) 34–48, https://doi.org/10.1002/anie.199100341.
[26] N.I. Gumerova, A. Rompel, Synthesis, structures and applications of electron-rich polyoxometalates, Nat. Rev. Chem. 2 (2018) 0112, https://doi.org/10.1038/s41570-018-0112.
[27] K. Nagai, H. Ichida, Y. Sasaki, The structure of heptapotassium tridecavanadomanganate (IV) octadecahydrate, $K_7MnV_{13}O_{38}{\cdot}18H_2O$, Chem. Lett. 15 (8) (1986) 1267–1270, https://doi.org/10.1246/cl.1986.1267.
[28] D.C. Crans, J.J. Smee, E. Gaidamauskas, L. Yang, J, Smee, E, Gaidamauskas, L, Yang, The chemistry and biochemistry of vanadium and the biological activities exerted by vanadium compounds, Chem. Rev. 104 (2) (2004) 849–902, https://doi.org/10.1021/cr020607t.
[29] "Vanadium" in Comprehensive Coordination Chemistry Reviews 2nd edition. Debbie C. Crans, and Jason J. Smee, 2004, 4.175-239, 10.1016/S0021-9258(19)86507-9.
[30] J. Costa Pessoa, I. Correia, Misinterpretations in evaluating interactions of vanadium complexes with proteins and other biological targets, Inorganics 917 (2021), https://doi.org/10.3390/inorganics9020017.
[31] D. Rehder (Ed.), Bioinorganic Vanadium Chemistry, John Wiley & Sons, Ltd, Chichester, UK, 2008.
[32] C. Amante, A.L. De Sousa-Coelho, M. Aureliano, Vanadium and melanoma: a systematic review, Metals 11 (2021) 828, https://doi.org/10.3390/met11050828.
[33] N.I. Gumerova, A. Rompel, Polyoxometalates in solution: speciation under spotlight, Chem. Soc. Rev. 49 (2020) 7568–7601, https://doi.org/10.1039/D0CS00392A.
[34] M. Aureliano, C.D. Crans, Decavanadate ($V_{10}O_{28}^{6-}$) and oxovanadates: Oxometalates with many biological activities, J. Inorg. Biochem. 103 (2009) 536–546, https://doi.org/10.1016/j.jinorgbio.2008.11.010.
[35] M. Aureliano, Decavanadate: a journey in a search of a role, Dalton Trans. (2009) 9093–9100, https://doi.org/10.1039/B907581J.
[36] H.T. Evans, The molecular structure of the isopoly complex ion, decavanadate ($V_{10}O_{28}^{6}$), Inorg. Chem. 5 (6) (1966) 967–977, https://doi.org/10.1021/ic50040a004.
[37] N. Bošnjaković-Pavlović, J. Prévost, A. Spasojević-de Biré, Crystallographic statistical study of decavanadate anion based-structures: toward a prediction of noncovalent interactions, Cryst. Growth Des. 11 (2011) 3778–3789, https://doi.org/10.1021/cg200236d.
[38] D.C. Crans, M. Mahroof-Tahir, O.P. Anderson, S.M. Miller, The X-ray structure of $(NH_4)_6(Gly\text{-}Gly)_2V_{10}O_{28}{\cdot}4H_2O$: model studies of polyoxometalate-protein interactions, Inorg. Chem. 44 (1994) 5586–5590, https://doi.org/10.1021/ic00102a036.
[39] S. Ramos, M. Manuel, T. Tiago, R.O. Duarte, J. Martins, C. Gutiérrez-Merino, J.J. G. Moura, M. Aureliano, Decavanadate interactions with actin inhibit G-actin polymerization and stabilize decameric vanadate species, J. Inorg. Biochem. 100 (2006) 1734–1743, https://doi.org/10.1016/j.jinorgbio.2006.06.007.
[40] R.M.C. Gândara, S.S. Soares, H. Martins, C. Gutiérrez-Merino, M. Aureliano, Vanadate oligomers: in vivo effects in hepatic vanadium accumulation and stress markers, J. Inorg. Biochem. 99 (2005) 1238–1244, https://doi.org/10.1016/j.jinorgbio.2005.02.023.
[41] H. Schmidt, I. Andersson, D. Rehder, L. Pettersson, A potentiometric and ^{51}V NMR study of the aqueous $H^+/H_2VO_4^-/H_2O_2$/L-α-alanyl-L-histidine system, Chem. Eur. J. 7 (2001) 251–257, https://doi.org/10.1002/1521-3765(20010105)7:1<251::AID-CHEM251>3.0.CO;2-9.
[42] M. Aureliano, R.M.C. Gândara, Decavanadate effects in biological systems, J. Inorg. Biochem. 99 (5) (2005) 979–985, https://doi.org/10.1016/j.jinorgbio.2005.02.024.
[43] L. Krivosudský, A. Roller, A. Rompel, Tuning the interactions of decavanadate with thaumatin, lysozyme, proteinase K and human serum proteins by its coordination to a pentaaquacobalt(II) complex cation, New J. Chem. 43 (2019) 17863–17871, https://doi.org/10.1039/C9NJ02495F.
[44] N. Samart, Z. Arhouma, S. Kumar, H.A. Murakami, D.C. Crick, D.C. Crans, Decavanadate inhibits microbacterial growth more potently than other oxovanadates, Front. Chem. 6 (2018) 519, https://doi.org/10.3389/fchem.
[45] D.C. Crans, E.M. Willging, S.R. Butler, Vanadate tetramer as inhibiting species in enzyme reactions *in vitro* and *in vivo*, J. Am. Chem. Soc. 112 (1990) 427–432, https://doi.org/10.1021/ja00157a063.
[46] D.C. Crans, K. Sudhakar, T.J. Zamborelli, Interaction of rabbit muscle aldolase at high ionic strengths with vanadate and other oxoanions, Biochemistry 31 (29) (1992) 6812–6821, https://doi.org/10.1021/bi00144a023.
[47] L. Wittenkeller, A. Abraha, R. Ramasamy, D. Mota de Freitas, L.A. Theisen, D.C. Crans, Vanadate interactions with bovine copper, zinc-superoxide dismutase as probed by ^{51}V NMR spectroscopy, J. Am. Chem. Soc. 113 (1991) 7872–7881, https://doi.org/10.1021/ja00021a008.
[48] D.C. Crans, C.M. Simone, A.K. Saha, R.H. Glew, Vanadate monomers and dimers both inhibit the human prostatic acid phosphatase, Biochem. Biophys. Res. Comm. 165 (1) (1989) 246–250, https://doi.org/10.1016/0006-291X(89)91061-9.
[49] T. Tiago, M. Aureliano, C. Gutiérrez-Merino, Decavanadate binding to a high affinity site near the myosin catalytic centre inhibits F-actin-stimulated myosin ATPase activity, Biochemistry 43 (18) (2004) 5551–5561, https://doi.org/10.1021/bi049910+.
[50] K. Kostenkova, Z. Arhouma, K. Postal, A. Rajan, U. Kortz, G.G. Nunes, D.C. Crick, D.C. Crans, Pt^{IV}- or Mo^{VI}-substituted decavanadates inhibit the growth of *Mycobacterium smegmatis*, J. Inorg. Biochem. 217 (2021) 111356, https://doi.org/10.1016/j.jinorgbio.2021.111356.
[51] A. Levina, D.C. Crans, P.A. Lay, Speciation of metal drugs, supplements and toxins in media and bodily fluids controls *in vitro* activities, Coord. Chem. Rev. 352 (2017) 473–498, https://doi.org/10.1016/j.ccr.2017.01.002.
[52] D.C. Crans, Aqueous chemistry of labile oxovanadates: Of relevance to biological studies, Comm. Inorg. Chem. 16 (1994) 1–33, https://doi.org/10.1080/02603599408035850.
[53] N.I. Gumerova, A. Rompel, Interweaving disciplines to advance chemistry: applying polyoxometalates in biology, Inorg. Chem. 60 (2021) 6109–6114, https://doi.org/10.1021/acs.inorgchem.1c00125.
[54] A.M. Silva-Nolasco, L. Camacho, R.O. Saavedra-Díaz, O. Hernández-Abreu, I.E. León, I. Sánchez-Lombardo, Kinetic studies of sodium and metforminium decavanadates decomposition and in vitro cytotoxicity and insulin-like activity, Inorganics 8 (2020) 67, https://doi.org/10.3390/inorganics8120067.
[55] S.S. Soares, M. Aureliano, N. Joaquim, J.M. Coucelo, Cadmium and vanadate oligomers effects on methaemoglobin reductase activity from Lusitanian

toadfish: in vivo and in vitro studies, J. Inorg. Biochem. 94 (3) (2003) 285–290, https://doi.org/10.1016/S0162-0134(03)00006-0.
[56] G. Fraqueza, C.André. Ohlin, W.H. Casey, M. Aureliano, Sarcoplasmic reticulum calcium ATPase interactions with decaniobate, decavanadate, vanadate, tungstate and molybdate, J. Inorg. Biochem. 107 (1) (2012) 82–89, https://doi.org/10.1016/j.jinorgbio.2011.10.010.
[57] G. Fraqueza, J. Fuentes, L. Krivosudský, S. Dutta, S.S. Mal, A. Roller, G. Giester, A. Rompel, M. Aureliano, Inhibition of Na^+/K^+- and Ca^{2+}-ATPase activities by phosphotetradecavanadate, J. Inorg. Biochem. 197 (2019) 110700, https://doi.org/10.1016/j.jinorgbio.2019.110700.
[58] B.M. Dorsey, C.C. McLauchlan, M.A. Jones, Evidence that speciation of oxovanadium complexes does not solely account for inhibition of *Leishmania* acid phosphatases, Front. Chem. 6 (2018) 109, https://doi.org/10.3389/fchem.2018.00109.
[59] M. Aureliano, C.André. Ohlin, M.O. Vieira, M.P.M. Marques, W.H. Casey, Luís.A. E. Batista de Carvalho, Characterization of decavanadate and decaniobate solutions by Raman spectroscopy, Dalton Trans. 45 (17) (2016) 7391–7399, https://doi.org/10.1039/C5DT04176G.
[60] J. Costa Pessoa, M.F.A. Santos, I. Correia, D. Sanna, G. Sciortino, E. Garribba, Binding of vanadium ions and complexes to proteins and enzymes in aqueous solution, Coord. Chem. Rev. 449 (2021) 214192, https://doi.org/10.1016/j.ccr.2021.214192.
[61] J. Costa Pessoa, E. Garribba, M.F.A. Santos, T. Santos-Silva, Vanadium and proteins: Uptake, transport, structure, activity and function, Coord. Chem. Rev. 301–302 (2015) 49–86, https://doi.org/10.1016/j.ccr.2015.03.016.
[62] C.H. Ng, C.W. Lim, S.G. Teoh, H.-K. Fun, A. Usman, S.W. Ng, New crown-shaped polyoxovanadium(V) cluster cation with a μ_6-sulfato anion and zwitterionic μ-(β-Alanine): crystal structure of $[V_6O_{12}(OH)_3(O_2CCH_2CH_2NH_3)_3(SO_4)][Na][SO_4]\cdot 13H_2O$, Inorg. Chem. 41 (2002) 2–3, https://doi.org/10.1021/ic015574z.
[63] S. Ramos, R.O. Duarte, J.J.G. Moura, M. Aureliano, Decavanadate interactions with actin: cysteine oxidation and vanadyl formation, Dalton Trans. (2009) 7985–7994, https://doi.org/10.1039/B906255F.
[64] G. Sciortino, M. Aureliano, E. Garribba, Rationalizing the decavanadate(V) and oxidovanadium(IV) binding to G-actin and the competition with decaniobate (V) and ATP, Inorg. Chem. 60 (1) (2021) 334–344, https://doi.org/10.1021/acs.inorgchem.0c0297110.1021/acs.inorgchem.0c02971.s001.
[65] G. Sciortino, D. Sanna, V. Ugone, J.-D. Maréchal, M. Alemany-Chavarria, E. Garribba, Effect of secondary interactions, steric hindrance and electric charge on the interaction of $V^{IV}O$ species with proteins, New J. Chem. 43 (45) (2019) 17647–17660, https://doi.org/10.1039/C9NJ01956A.
[66] A. Banerjee, S.P. Dash, M. Mohanty, G. Sahu, G. Sciortino, E. Garribba, M.F.N.N. Carvalho, F. Marques, J. Costa Pessoa, W. Kaminsky, K. Brzezinski, R. Dinda, New V^{IV}, $V^{IV}O$, $V^{V}O$, and $V^{V}O_2$ Systems: Exploring their interconversion in Solution, Protein Interactions, and Cytotoxicity, Inorg. Chem. 59 (2020) 14042–14057, https://doi.org/10.1021/acs.inorgchem.0c01837.
[67] M. Arefian, M. Mirzaei, H. Eshtiagh-Hosseini, A. Frontera, A survey of the different roles of polyoxometalates in their interaction with amino acids, peptides and proteins, Dalton Trans. 46 (21) (2017) 6812–6829, https://doi.org/10.1039/C7DT00894E.
[68] V. Ugone, D. Sanna, S. Ruggiu, G. Sciortino, E. Garribba, Covalent and non-covalent binding in vanadium–protein adducts, Inorg. Chem. Front. 8 (5) (2021) 1189–1196, https://doi.org/10.1039/D0QI01308K.
[69] G. Sciortino, J.-D. Maréchal, E. Garribba, Integrated approaches to characterize the systems formed by vanadium with proteins and enzymes, Inorg. Chem. Front. 8 (2021) 1951–1974, https://doi.org/10.1039/D0QI01507E.
[70] R.A. Friesner, J.L. Banks, R.B. Murphy, T.A. Halgren, J.J. Klicic, D.T. Mainz, M.P. Repasky, E.H. Knoll, M. Shelley, J.K. Perry, D.E. Shaw, P. Francis, P.S. Shenkin, Glide: a new approach for rapid, accurate docking and scoring. 1. Method and assessment of docking accuracy, J. Med. Chem. 47 (2004) 1739–1749, https://doi.org/10.1021/jm0306430.
[71] G.M. Morris, R. Huey, W. Lindstrom, M.F. Sanner, R.K. Belew, D.S. Goodsell, A.J. Olson, AutoDock4 and AutoDockTools4: automated docking with selective receptor flexibility, J. Comput. Chem. 30 (2009) 2785–2791, https://doi.org/10.1002/jcc.21256.
[72] C.R. Corbeil, C.I. Williams, P. Labute, Variability in docking success rates due to dataset preparation, J. Comput.-Aided Mol. Des. 26 (6) (2012) 775–786, https://doi.org/10.1007/s10822-012-9570-1.
[73] E. Ortega-Carrasco, A. Lledós, J.-D. Maréchal, Assessing protein–ligand docking for the binding of organometallic compounds to proteins, J. Comput. Chem. 35 (3) (2014) 192–198, https://doi.org/10.1002/jcc.23472.
[74] G. Sciortino, D. Sanna, V. Ugone, A. Lledós, J.-D. Maréchal, E. Garribba, Decoding surface interaction of $V^{IV}O$ metallodrug candidates with lysozyme, Inorg. Chem. 57 (8) (2018) 4456–4469, https://doi.org/10.1021/acs.inorgchem.8b00134.
[75] G. Jones, P. Willett, R.C. Glen, A.R. Leach, R. Taylor, Development and validation of a genetic algorithm for flexible docking, J. Mol. Biol. 267 (1997) 727–748, https://doi.org/10.1006/jmbi.1996.0897.
[76] X. Ouyang, S. Zhou, C.T.T. Su, Z. Ge, R. Li, C.K. Kwoh, CovalentDock: Automated covalent docking with parameterized covalent linkage energy estimation and molecular geometry constraints, J. Comput. Chem. 34 (2013) 326–336, https://doi.org/10.1002/jcc.23136.
[77] C. Scholz, S. Knorr, K. Hamacher, B. Schmidt, DOCKTITE — a highly versatile step-by-step workflow for covalent docking and virtual screening in the molecular operating environment, J. Chem. Inf. Model. 55 (2) (2015) 398–406, https://doi.org/10.1021/ci500681r.
[78] G. Sciortino, E. Garribba, J.-D. Maréchal, Validation and applications of protein–ligand docking approaches improved for metalloligands with multiple vacant sites, Inorg. Chem. 58 (1) (2019) 294–306, https://doi.org/10.1021/acs.inorgchem.8b02374.
[79] G. Sciortino, J. Rodriguez-Guerra Pedregal, A. Lledos, E. Garribba, J.D. Marechal, Prediction of the interaction of metallic moieties with proteins: an update for protein-ligand docking techniques, J. Comput. Chem. 39 (2018) 42–51, https://doi.org/10.1002/jcc.25080.
[80] E.G. DeMaster, R.A. Mitchell, A comparison of arsenate and vanadate as inhibitors or uncouplers of mitochondrial and glycolytic energy metabolism, Biochemistry 12 (19) (1973) 3616–3621, https://doi.org/10.1021/bi00743a007.
[81] D.W. Boyd, K. Kustin, M. Niwa, Do vanadate polyanions inhibit phosphotransferase enzymes?, Biochim Biophys. Acta (BBA) Protein Struct. Mol. Enzymol. 827 (3) (1985) 472–475, https://doi.org/10.1016/0167-4838(85)90235-3.
[82] G. Choate, T.E. Mansour, Studies on heart phosphofructokinase. Decavanadate as a potent allosteric inhibitor at alkaline and acidic pH, J. Biol. Chem. 254 (22) (1979) 11457–11462, https://doi.org/10.1016/S0021-9258(19)86507-9.
[83] G. Soman, Y.C. Chang, D.J. Graves, Effect of oxyanions of the early transition metals on rabbit skeletal muscle phosphorylase, Biochemistry 22 (21) (1983) 4994–5000, https://doi.org/10.1021/bi00290a018.
[84] P. Csermely, A. Martonosi, G.C. Levy, A.J. Ejchart, ^{51}V-n.m.r. analysis of the binding of vanadium(V) oligoanions to sarcoplasmic reticulum, Biochem. J. 230 (1985) 807–815, https://doi.org/10.1042/bj2300807.
[85] M. Aureliano, V.M.C. Madeira, Interactions of vanadate oligomers with sarcoplasmic reticulum Ca^{2+}-ATPase, Biochim. Biophys. Acta 1221 (3) (1994) 259–271, https://doi.org/10.1016/0167-4889(94)90249-6.
[86] M. Aureliano, V.M. Madeira, Vanadate oligoanions interact with the proton ejection by the Ca^{2+} pump of sarcoplasmic reticulum, Biochem. Biophys. Res. Commun. 205 (1994) 161–167, https://doi.org/10.1006/bbrc.1994.2644.
[87] M. Aureliano, V.M.C. Madeira, Energy transduction systems as affected by vanadate oligomers: sarcoplasmic reticulum calcium pump, in: J.O. Nriagu (Ed.), Vanadium in the environment, Part 1: Chemistry and Biochemistry, John Wiley & Sons Inc, New York, 1998, pp. 333–358.
[88] D.C. Crans, Interactions of oxovanadates and selected oxomolybdates with proteins, Mol. Eng. 3 (1-3) (1993) 277–284, https://doi.org/10.1007/BF00999638.
[89] D.C. Crans, S.M. Schelble, Vanadate dimer and tetramer both inhibit glucose-6-phosphate dehydrogenase from *Leuconostoc mesenteroides*, Biochemistry 29 (28) (1990) 6698–6706, https://doi.org/10.1021/bi00480a020.
[90] L. Wittenkeller, A. Abraha, R. Ramasamy, D.M. De Freitas, L.A. Theisen, D.C. Crans, Vanadate interactions with bovine copper, zinc-superoxide dismutase as probed by vanadium-51 NMR spectroscopy, J. Am. Chem. Soc. 113 (21) (1991) 7872–7881, https://doi.org/10.1021/ja00021a008.
[91] S. Pluskey, M. Mahroof-Tahir, D.C. Crans, D.S. Lawrence, Vanadium oxoanions and cAMP-dependent protein kinase: An anti-substrate inhibitor, Biochem. J. 321 (1997) 333–339, https://doi.org/10.1042/bj3210333.
[92] R.J. Pezza, M.A. Villarreal, G.G. Montich, C.E. Argaraña, Vanadate inhibits the ATPase activity and DNA binding capability of bacterial MutS. A structural model for the vanadate-MutS interaction at the Walker A motif, Nucleic Acids Res. 30 (2002) 4700–4708, https://doi.org/10.1093/nar/gkf606.
[93] D.C. Crans, M.L. Tarlton, C.C. McLauchlan, Trigonal bipyramidal or square pyramidal coordination geometry? investigating the most potent geometry for vanadium phosphatase inhibitors, Eur. J. Inorg. Chem. 2014 (27) (2014) 4450–4468, https://doi.org/10.1002/ejic.201402306.
[94] C.C. McLauchlan, B.J. Peters, G.R. Willsky, D.C. Crans, Vanadium-protein complexes: phosphatase inhibitors favor the trigonal bipyramidal transition state geometries, Coord. Chem. Rev. 301–302 (2015) 163–199, https://doi.org/10.1016/j.ccr.2014.12.012.
[95] S.R. Akabayov, B. Akabayov, Vanadate in structural biology, Inorg. Chim. Acta 420 (2014) 16–23, https://doi.org/10.1016/j.ica.2014.02.010.
[96] D.R. Davies, W.G.J. Hol, The power of vanadate in crystallographic investigations of phosphoryl transfer enzymes, FEBS Lett. 577 (2004) 315–321, https://doi.org/10.1016/j.febslet.2004.10.022.
[97] D.C. Crans, C.M. Simone, Nonreductive interaction of vanadate with an enzyme containing a thiol group in the active site: Glycerol-3-phosphate dehydrogenase, Biochemistry 30 (1991) 6734–6741, https://doi.org/10.1021/bi00241a015.
[98] D.C. Crans, C.M. Simone, R.C. Holz, L. Que, Interaction of porcine uterine fluid purple acid phosphatase with vanadate and vanadyl cation, Biochemistry 31 (47) (1992) 11731–11739, https://doi.org/10.1021/bi00162a009.
[99] T. Tiago, M. Aureliano, J.J.G. Moura, Decavanadate as a biochemical tool in the elucidation of muscle contraction regulation, J. Inorg. Biochem. 98 (11) (2004) 1902–1910, https://doi.org/10.1016/j.jinorgbio.2004.08.013.
[100] L. Csanady, V. Adam-Vizi, Antagonistic regulation of native Ca^{2+}- and ATP-sensitive cation channels in brain capillaries by nucleotides and decavanadate, J. Gen. Physiol. 123 (2004) 743–757, https://doi.org/10.1085/jgp.200309008.
[101] B. Nilius, J. Prenen, A. Janssens, T. Voets, G. Droogmans, Decavanadate modulates gating of TRPM4 cation channels, J. Physiol. 560 (2004) 753–765, https://doi.org/10.1113/jphysiol.2004.070839.
[102] I. Bougie, M. Bisaillon, Inhibition of a metal-dependent viral RNA triphosphatase by decavanadate, Biochem. J. 398 (2006) 557–567, https://doi.org/10.1042/BJ20060198.

[103] A.D. Michel, M. Xing, K.M. Thompson, C.A. Jones, P.P.A. Humphrey, Decavanadate, a P2X receptor antagonist, and its use to study ligand interactions with $P2X_7$ receptors, Eur. J. Pharmacol. 534 (1-3) (2006) 19–29, https://doi.org/10.1016/j.ejphar.2006.01.009.
[104] T. Tiago, P. Martel, C. Gutiérrez-Merino, M. Aureliano, Binding modes of decavanadate to myosin and inhibition of the actomyosin ATPase activity, Biochim. Biophys. Acta 1774 (4) (2007) 474–480, https://doi.org/10.1016/j.bbapap.2007.02.004.
[105] M. Gutiérrez-Aguilar, V. Pérez-Vázquez, O. Bunoust, S. Manon, M. Rigoulet, S. Uribe, In yeast, Ca^{2+} and octylguanidine interact with porin (VDAC) preventing the mitochondrial permeability transition, Biochim. Biophys. Acta 1767 (10) (2007) 1245–1251, https://doi.org/10.1016/j.bbabio.2007.07.002.
[106] S.S. Soares, C. Gutiérrez-Merino, M. Aureliano, Decavanadate induces mitochondrial membrane depolarization and inhibits oxygen consumption, J. Inorg. Biochem. 101 (5) (2007) 789–796, https://doi.org/10.1016/j.jinorgbio.2007.01.012.
[107] D. Krstić, M. Colović, N. Bosnjaković-Pavlović, A. Spasojević-De Bire, V. Vasić, Influence of decavanadate on rat synaptic plasma membrane ATPases activity, Gen. Physiol. Biophys. 28 (2009) 302–308, https://doi.org/10.4149/gpb_2009_03_302.
[108] A. Al-Qatati, F.L. Fontes, B.G. Barisas, D. Zhang, D.A. Roess, D.C. Crans, Raft localization of Type I Fc epsilon receptor and degranulation of RBL-2H3 cells exposed to decavanadate, a structural model for V_2O_5, Dalton Trans. 42 (2013) 11912–11920, https://doi.org/10.1039/C3DT50398D.
[109] M.P.M. Marques, D. Gianolio, S. Ramos, L.A.E. Batista de Carvalho, M. Aureliano, An EXAFS approach to the study of polyoxometalate-protein interactions: The case of decavanadate-actin, Inorg. Chem. 56 (18) (2017) 10893–10903, https://doi.org/10.1021/acs.inorgchem.7b01018.
[110] D. Marques-Da-Silva, G. Fraqueza, R. Lagoa, A.A. Vannathan, S.S. Mal, M. Aureliano, Polyoxovanadate inhibition of: *Escherichia coli* growth shows a reverse correlation with Ca^{2+}-ATPase inhibition, New J. Chem. 43 (2019) 17577–17587, https://doi.org/10.1039/C9NJ01208G.
[111] H.M. Berman, K. Henrick, H. Nakamura, Announcing the worldwide Protein Data Bank, Nature Struct. Biol. 10 (12) (2003) 980, https://doi.org/10.1038/nsb1203-980.
[112] www.wwpdb.org.
[113] A.S. Arvai, Y. Bourne, M.J. Hickey, J.A. Tainer, Crystal structure of the human cell cycle protein cksh1: single domain fold with similarity to kinase n-lobe domain, J. Mol. Biol. 249 (1995) 835–842, https://doi.org/10.1006/jmbi.1995.0341.
[114] R.L. Felts, T.J. Reilly, J.J. Tanner, Structure of *Francisella tularensis* AcpA: prototype of a unique superfamily of acid phosphatases and phospholipases C, J. Biol. Chem. 6 (2006) 30289–30298, https://doi.org/10.1074/jbc.M606391200.
[115] Q.Q. Zheng, D.Q. Jiang, W. Zhang, Q.Q. Zhang, J. Jin, X. Li, H.T. Yang, N. Shaw, W. Zhou, Z. Rao, unpublished work, http://doi.org/10.2210/pdb4qih/pdb.
[116] S.C. Robson, J. Sévigny, H. Zimmermann, The E-NTPDase family of ectonucleotidases: Structure function relationships and pathophysiological significance, Purinergic Signal. 2 (2006) 409–430, https://doi.org/10.1007/s11302-006-9003-5.
[117] T.T. Caradoc-Davies, S.M. Cutfield, I.L. Lamont, J.F. Cutfield, Crystal structures of *Escherichia coli* uridine phosphorylase in two native and three complexed forms reveal basis of substrate specificity, induced conformational changes and influence of potassium, J. Mol. Biol. 337 (2) (2004) 337–354, https://doi.org/10.1016/j.jmb.2004.01.039.
[118] C.C. McLauchlan, H.A. Murakami, C.A. Wallace, D.C. Crans, Coordination environment changes of the vanadium in vanadium-depending haloperoxidase enzymes, J. Inorg. Biochem. 186 (2018) 267–279, https://doi.org/10.1016/j.jinorgbio.2018.06.011.
[119] M. Zebisch, M. Krauss, P. Schäfer, N. Sträter, Crystallographic evidence for a domain motion in rat nucleoside triphosphate diphosphohydrolase (NTPDase) 1, J. Mol. Biol. 415 (2) (2012) 288–306, https://doi.org/10.1016/j.jmb.2011.10.050.
[120] M. Zebisch, M. Krauss, P. Schäfer, P. Lauble, N. Sträter, Crystallographic snapshots along the reaction pathway of nucleoside triphosphate diphosphohydrolases, Structure 21 (8) (2013) 1460–1475, https://doi.org/10.1016/j.str.2013.05.016.
[121] J.H. Bae, E.D. Lew, S. Yuzawa, F. Tomé, I. Lax, J. Schlessinger, The selectivity of receptor tyrosine kinase signaling is controlled by a secondary SH2 domain binding site, Cell 138 (3) (2009) 514–524, https://doi.org/10.1016/j.cell.2009.05.028.
[122] Z. Du, C.M. Lovly, Mechanisms of receptor tyrosine kinase activation in cancer, Mol Cancer. 17 (2018) 58, https://doi.org/10.1186/s12943-018-0782-4.
[123] N. Samart, D. Althumairy, D. Zhang, D.A. Roess, D.C. Crans, Initiation of a novel mode of membrane signaling: vanadium facilitated signal transduction, Coord. Chem. Rev. 416 (2020) 213–286, https://doi.org/10.1016/j.ccr.2020.213286.
[124] D.C. Crans, K.A. Woll, K. Prusinskas, M.D. Johnson, E. Norkus, Metal speciation in health and medicine represented by iron and vanadium, Inorg. Chem. 52 (2013) 12264–12275, https://doi.org/10.1021/ic4007873.
[125] A. Chatkon, P.B. Chatterjee, M.A. Sedgwick, K.J. Haller, D.C. Crans, Counterion affects interaction with interfaces: The antidiabetic drugs metformin and decavanadate, Eur. J. Inorg. Chem. 2013 (2013) 1859–1868, https://doi.org/10.1002/ejic.201201345.
[126] P.A. Winkler, Y. Huang, W. Sun, J. Du, W. Lü, Electron cryo-microscopy structure of a human TRPM4 channel, Nature 552 (7684) (2017) 200–204, https://doi.org/10.1038/nature24674.
[127] K.L. Gould, P. Nurse, Tyrosine phosphorylation of the fission yeast *cdc2*$^+$ protein kinase regulates entry into mitosis, Nature 342 (6245) (1989) 39–45, https://doi.org/10.1038/342039a0.
[128] H.E. Richardson, C.S. Stueland, J. Thomas, P. Russell, S.I. Reed, Human cDNAs encoding homologs of the small p34Cdc28/cdc2-associated protein of *Saccharomyces cerevisiae* and *Schizosaccharomyces pombe*, Genes & Dev. 4 (1990) 1332–1344, https://doi.org/10.1101/gad.4.8.1332.
[129] C.S. Bond, M.F. White, W.N. Hunter, Mechanistic implications for *Escherichia coli* cofactor-dependent phosphoglycerate mutase based on the high-resolution crystal structure of a vanadate complex, J. Mol. Biol. 316 (5) (2002) 1071–1081, https://doi.org/10.1006/jmbi.2002.5418.
[130] E. Heath, O.W. Howarth, Vanadium-51 and oxygen-17 nuclear magnetic resonance study of vanadate(V) equilibria and kinetics, J. Chem. Soc., Dalton Trans. (1981) 1105–1110, https://doi.org/10.1039/DT9810001105.
[131] H.R. Evans, D.E. Holloway, J.M. Sutton, J. Ayriss, C.C. Shone, K.R. Acharya, C3 exoenzyme from *Clostridium botulinum*: structure of a tetragonal crystal form and a reassessment of NAD-induced flexure, Acta Crystallogr. D Biol. Crystallogr. 60 (8) (2004) 1502–1505, https://doi.org/10.1107/S0907444904011680.
[132] K.P. Locher, A.T. Lee, D.C. Rees, E. The, *coli* BtuCD structure: A framework for ABC transporter architecture and mechanism, Science 296 (2002) 1091–1098, https://doi.org/10.1126/science.1071142.
[133] D.J. Rigden, J.E. Littlejohn, K. Henderson, M.J. Jedrzejas, Structures of phosphate and trivanadate complexes of *Bacillus stearothermophilus* phosphatase PhoE: structural and functional analysis in the cofactor-dependent phosphoglycerate mutase superfamily, J. Mol. Biol. 325 (2003) 411–420, https://doi.org/10.1016/s0022-2836(02)01229-9.
[134] T.A.S. Brandão, H. Robinson, S.J. Johnson, A.C. Hengge, Impaired acid catalysis by mutation of a protein loop hinge residue in a YopH mutant revealed by crystal structures, J. Am. Chem. Soc. 131 (2) (2009) 778–786, https://doi.org/10.1021/ja807418b.
[135] D.C. Crans, P.K. Shin, Spontaneous and reversible interactions of vanadium(V) oxyanions with amine derivatives, Inorg. Chem. 27 (1988) 1797–1806, https://doi.org/10.1021/ic00283a025.
[136] D.C. Crans, R.L. Bunch, L.A. Theisen, Interaction of trace levels of vanadium (IV) and (V) in biological systems, J. Am. Chem. Soc. 111 (1989) 7597–7607, https://doi.org/10.1021/ja00201a049.
[137] S.G. Mauracher, C. Molitor, R. Al-Oweini, U. Kortz, A. Rompel, Crystallization and preliminary X-ray crystallographic analysis of latent isoform PPO4 mushroom (*Agaricus bisporus*) tyrosinase, Acta Cryst. F 70 (2014) 263–266, https://doi.org/10.1107/S2053230X14000582.
[138] S.G. Mauracher, C. Molitor, R. Al-Oweini, U. Kortz, A. Rompel, Latent and active *ab*PPO4 mushroom tyrosinases cocrystallized with hexatungstotellurate(VI) in a single crystal, Acta Cryst. D 70 (2014) 2301–2315, https://doi.org/10.1107/S1399004714013777.
[139] C. Molitor, A. Bijelic, A. Rompel, *In situ* formation of the first proteinogenically functionalized $[TeW_6O_{24}O_2(Glu)]^{7-}$ structure reveals unprecedented chemical and geometrical features of the Anderson-type cluster, Chem. Commun. 52 (83) (2016) 12286–12289, https://doi.org/10.1039/C6CC07004C.
[140] C. Molitor, A. Bijelic, A. Rompel, The potential of hexatungstotellurate(VI) to induce a significant entropic gain during protein crystallization, IUCrJ 4 (6) (2017) 734–740, https://doi.org/10.1107/S205225251701234910.1107/S2052252517012349/lq5006sup1.pdf.
[141] A. Bijelic, A. Rompel, Ten good reasons for the use of the Tellurium-centered Anderson-Evans polyoxotungstate in protein crystallography, Acc. Chem. Res. 50 (2017) 1441–1448, https://doi.org/10.1021/acs.accounts.7b00109.
[142] W.J. Ray, D.C. Crans, J. Zheng, J.W. Burgner II, H. Deng, M. Mahroof-Tahir, Structure of the dimeric ethylene glycol- vanadate complex and other 1,2-diol-vanadate complexes in aqueous solution. Vanadate-based transition state analog complexes of phosphotransferases, J. Am. Chem. Soc. 117 (1995) 6015–6026, https://doi.org/10.1021/ja00127a015.
[143] U. Pick, The interaction of vanadate ions with the Ca-ATPase from sarcoplasmic reticulum, J. Biol. Chem. 257 (1982) 6111–6119, https://doi.org/10.1016/S0021-9258(20)65113-4.
[144] S. Ramos, J.J.G. Moura, M. Aureliano, Actin as a potential target for decavanadate, J. Inorg. Biochem. 104 (12) (2010) 1234–1239, https://doi.org/10.1016/j.jinorgbio.2010.08.001.
[145] M. Aureliano, M.C. Pedroso de Lima and E.M.V. Pires, Inhibition of Actomyosin MgATPase by Decavanadate: A Flow Microcalorimetry Study". III Congreso Luso-Español de Bioquimica, 12-16 September 1988, Santiago de Compostela, Spain.
[146] A. Ścibior, Ł. Pietrzyk, Z. Plewa, A. Skiba, Vanadium: Risks and possible benefits in the light of a comprehensive overview of its pharmacotoxicological mechanisms and multi-applications with a summary of further research trends, J. Trace Elem. Med. Biol. 61 (2021) 126508, https://doi.org/10.1016/j.jtemb.2020.126508.
[147] R.T. MacGillivray, E. Mendez, J.G. Shewale, S.K. Sinha, J. Lineback-Zins, K. Brew, The primary structure of human serum transferrin. The structures of seven cyanogen bromide fragments and the assembly of the complete structure, J. Biol. Chem. 258 (1983) 3543–3553, https://doi.org/10.1016/S0021-9258(18)32696-6.

[148] J. Schaller, S. Gerber, U. Kämpfer, S. Lejon, C. Trachsel, in: Human blood plasma proteins: structure and function, John Wiley & Sons Ltd., Chichester, 2008, https://doi.org/10.1002/9780470724378.
[149] R. Crichton, Iron Metabolism - From Molecular Mechanisms to Clinical Consequences, 3rd Edition., John Wiley & Sons Ltd, Chichester, 2009.
[150] J.A. Benjamín-Rivera, A.E. Cardona-Rivera, Á.L. Vázquez-Maldonado, C.Y. Dones-Lassalle, H.L. Pabón-Colon, H.M. Rodríguez-Rivera, I. Rodríguez, J.C. González-Espiet, J. Pazol, J.D. Pérez-Ríos, J.F. Catala-Torres, M. Carrasquillo Rivera, M.G. De Jesus-Soto, N.A. Cordero-Virella, P.M. Cruz-Maldonado, P. González-Pagan, R. Hernández-Ríos, K. Gaur, S.A. Loza-Rosas, Exploring serum transferrin regulation of nonferric metal therapeutic function and toxicity, Inorganics 8 (2020) 48, https://doi.org/10.3390/inorganics8090048.
[151] J. Williams, K. Moreton, The distribution of iron between the metal-binding sites of transferrin human serum, Biochem. J. 185 (1980) 483–488, https://doi.org/10.1042/bj1850483.
[152] W. Bal, M. Sokołowska, E. Kurowska, P. Faller, Binding of transition metal ions to albumin: Sites, affinities and rates, Biochim. Biophys. Acta, Gen. Subj. 1830 (12) (2013) 5444–5455, https://doi.org/10.1016/j.bbagen.2013.06.018.
[153] S. Al-Harthi, J.I. Lachowicz, M.E. Nowakowski, M. Jaremko, Ł. Jaremko, Towards the functional high-resolution coordination chemistry of blood plasma human serum albumin, J. Inorg. Biochem. 198 (2019) 110716, https://doi.org/10.1016/j.jinorgbio.2019.110716.
[154] World health organization, Diabetes statistic. <https://www.who.int/news-room/fact-sheets/detail/diabetes>, 2021 (accessed September 29, 2021).
[155] H. Sakurai, A new concept: the use of vanadium complexes in the treatment of diabetes mellitus, Chem. Rec. 2 (2002) 237–248, https://doi.org/10.1002/tcr.10029.
[156] M. Melchior, S.J. Rettig, B.D. Liboiron, K.H. Thompson, V.G. Yuen, J.H. McNeill, C. Orvig, Insulin-enhancing vanadium(III) complexes, Inorg. Chem. 40 (18) (2001) 4686–4690, https://doi.org/10.1021/ic000984t.
[157] B. Lyonnet, X. Martz, E. Martin, L'emploi thérapeutique des dérivés du vanadium, La Presse Medicale 32 (1899) 191–192.
[158] K.H. Thompson, J.H. McNeill, C. Orvig, Vanadium compounds as insulin mimics, Chem. Rev. 99 (9) (1999) 2561–2572, https://doi.org/10.1021/cr980427c.
[159] E.L. Tolman, E. Barris, M. Burns, A. Pansini, R. Partridge, Effects of vanadium on glucose metabolism *in vitro*, Life Sci. 25 (13) (1979) 1159–1164, https://doi.org/10.1016/0024-3205(79)90138-3.
[160] Y. Shechter, S.J.D. Karlish, Insulin-like stimulation of glucose oxidation in rat adipocytes by vanadyl (IV) ions, Nature 284 (5756) (1980) 556–558, https://doi.org/10.1038/284556a0.
[161] D.C. Crans, L. Henry, G. Cardiff, G. Posner, Developing vanadium as an antidiabetic drug: A clinical and historical perspective, Met. Ions Life Sci. 19 (2019) 203–230, https://doi.org/10.1515/9783110527872-014.
[162] G.R. Willsky, L.-H. Chi, M. Godzala, P.J. Kostyniak, J.J. Smee, A.M. Trujillo, J.A. Alfano, W. Ding, Z. Hu, D.C. Crans, Anti-diabetic effects of a series of vanadium dipicolinate complexes in rats with Streptozotocin induced diabetes, Coord. Chem. Rev. 255 (19-20) (2011) 2258–2269, https://doi.org/10.1016/j.ccr.2011.06.015.
[163] K. Nomiya, H. Torii, T. Hasegawa, Y. Nemoto, K. Nomura, K. Hashino, M. Uchida, Y. Kato, K. Shimizu, M. Oda, Insulin mimetic effect of tungstate cluster. Effect of oral administration of homo-polyoxotungstates and vanadium-substituted polyoxotungstates on blood glucose level of STZ mice, J. Inorg. Biochem. 86 (2001) 657–667, https://doi.org/10.1016/s0162-0134(01)00233-1.
[164] E. Sánchez-Lara, S. Treviño, B.L. Sánchez-Gaytán, E. Sánchez-Mora, M.E. Castro, F.J. Meléndez-Bustamante, M.A. Méndez-Rojas, E. González-Vergara, Decavanadate salts of cytosine and metformin: A combined experimental-theoretical study of potential metallodrugs against diabetes and cancer, Front. Chem. 6 (2018) 402, https://doi.org/10.3389/fchem.2018.00402.
[165] S.S. Soares, F. Henao, M. Aureliano, C. Gutiérrez-Merino, Vanadate-induced necrotic death in neonatal rat cardiomyocytes through mitochondrial membrane depolarization, Chem. Res. Toxicol. 21 (2008) 607–618, https://doi.org/10.1021/tx700204r.
[166] Ş. Bâlici, M. Wankeu-Nya, D. Rusu, G.Z. Nicula, M. Rusu, A. Florea, H. Matei, Ultrastructural analysis of *In Vivo* hypoglycemiant effect of two polyoxometalates in rats with streptozotocin-induced diabetes, Microscopy and Microanalysis 21 (5) (2015) 1236–1248, https://doi.org/10.1017/S1431927615015020.
[167] S. Treviño, A. Díaz, E. Sánchez-Lara, B.L. Sanchez-Gaytan, J.M. Perez-Aguilar, E. González-Vergara, Vanadium in biological action: Chemical, pharmacological aspects, and metabolic implications in diabetes mellitus, Biol. Trace Elem. Res. 188 (2019) 68–98, https://doi.org/10.1007/s12011-018-1540-6.
[168] S. Treviño, E. González-Vergara, Metformin-decavanadate treatment ameliorates hyperglycemia and redox balance of the liver and muscle in a rat model of alloxan-induced diabetes, New J. Chem. 43 (2019) 17850–17862, https://doi.org/10.1039/C9NJ02460C.
[169] G. Chi, Y. Qi, J. Li, L. Wang, J. Hu, Polyoxomolybdates as α-glucosidase inhibitors: kinetic and molecular modeling studies, J. Inorg. Biochem. 193 (2019) 173–179, https://doi.org/10.1016/j.jinorgbio.2019.02.001.
[170] G. Chi, L. Wang, B. Chen, J. Li, J. Hu, S. Liu, M. Zhao, X. Ding, Y. Li, Polyoxometalates: Study of inhibitory kinetics and mechanism against α-glucosidase, J. Inorg. Biochem. 199 (2019) 110784, https://doi.org/10.1016/j.jinorgbio.2019.110784.
[171] J. Hu, L. Wang, F. Wang, G. Chi, G. Liu, L. Sun, Molecular docking of polyoxometalates as potential α-glucosidase inhibitors, J. Inorg. Biochem. 203 (2020) 110914, https://doi.org/10.1016/j.jinorgbio.2019.110914.
[172] M. Kazmi, S. Zaib, A. Ibrar, S.T. Amjad, Z. Shafique, S. Mehsud, A. Saeed, J. Iqbal, I. Khan, A new entry into the portfolio of α-glucosidase inhibitors as potent therapeutics for type 2 diabetes: design, bioevaluation and one-pot multi-component synthesis of diamine-bridged coumarinyl oxadiazole conjugates, Bioorg. Chem. 77 (2018) 190–202, https://doi.org/10.1016/j.bioorg.2017.12.022.
[173] J.-J. Hu, L. Wang, B.-N. Chen, G.-X. Chi, M.-J. Zhao, Y. Li, Transition metal substituted polyoxometalates as α-glucosidase inhibitors, Eur. J. Inorg. Chem. 2019 (2019) 3270–3276, https://doi.org/10.1002/ejic.201900306.
[174] W. Legrum, The mode of reduction of vanadate(+V) to oxovanadium(+IV) by glutathione and cysteine, Toxicology 42 (1986) 281–289, https://doi.org/10.1016/0300-483X(86)90016-8.
[175] L. Capella, M. Gefé, E. Silva, E. Affonso-Mitidieri, A. Lopes, V. Rumjanek, M. Capella, Mechanisms of vanadate-induced cellular toxicity: role of cellular glutathione and NADPH, Arch. Biochem. Biophys. 406 (2002) 65–72, https://doi.org/10.1016/S0003-9861(02)00408-3.
[176] Z. Zhang, S. Leonard, C. Huang, V. Vallyathan, V. Castranova, X. Shi, Role of reactive oxygen species and MAPKS in vanadate-induced G(2)/M phase arrest, Free Radic. Biol. Med. 34 (2003) 1333–1342, https://doi.org/10.1016/S0891-5849(03)00145-X.
[177] S.J. Stohs, D. Bagchi, Oxidative mechanisms in the toxicity of metal ions, Free Radic. Biol. Med. 18 (1995) 321–336, https://doi.org/10.1016/0891-5849(94)00159-H.
[178] J.Z. Byczkowski, A.P. Kulkarni, Oxidative stress and pro-oxidant biological effects of vanadium, in: J.O. Nriagu (Ed.), Vanadium in the environment, Part 1: Chemistry and Biochemistry, John Wiley & Sons Inc, New York, 1998, pp. 235–263.
[179] M. Aureliano, N. Joaquim, A. Sousa, H. Martins, J.M. Coucelo, Oxidative stress in toadfish (*Halobactrachus didactylus*) cardiac muscle: Acute exposure to vanadate oligomers, J. Inorg. Biochem. 90 (2002) 159–165, https://doi.org/10.1016/S0162-0134(02)00414-2.
[180] G. Borges, P. Mendonça, N. Joaquim, M. Aureliano, J.M. Coucelo, Acute effects of vanadate oligomers on heart, kidney, and liver histology in the Lusitanian toadfish (*Halobatrachus didactylus*), Arch. Environ. Contam. Toxicol. 45 (2003) 415–422, https://doi.org/10.1007/s00244-003-2155-1.
[181] S. Soares, H. Martins, R. Duarte, J.J.G. Moura, J.M. Coucelo, C. Gutiérrez-Merino, M. Aureliano, Vanadium distribution, lipid peroxidation and oxidative stress markers upon decavanadate *in vivo* administration, J. Inorg. Biochem. 101 (2007) 80–88, https://doi.org/10.1016/j.jinorgbio.2006.08.002.
[182] M. Aureliano, C.A. Ohlin, Decavanadate *in vitro* and *in vivo* effects: facts and opinions, J. Inorg. Biochem. 137 (2014) 123–130, https://doi.org/10.1016/j.jinorgbio.2014.05.002.
[183] S. Soares, H. Martins, M. Aureliano, Vanadium distribution dependence on decavanadate administration, Arch. Environ. Contam. Toxicol. 50 (2006) 60–64, https://doi.org/10.1007/s00244-004-0246-2.